Graphical Abstract

A comparative study of the atmospheric water vapor in the Atacama and Namib Desert

Jose Vicencio Veloso, Christoph Böhm, Jan H. Schween, Ulrich Löhnert, and Susanne Crewell

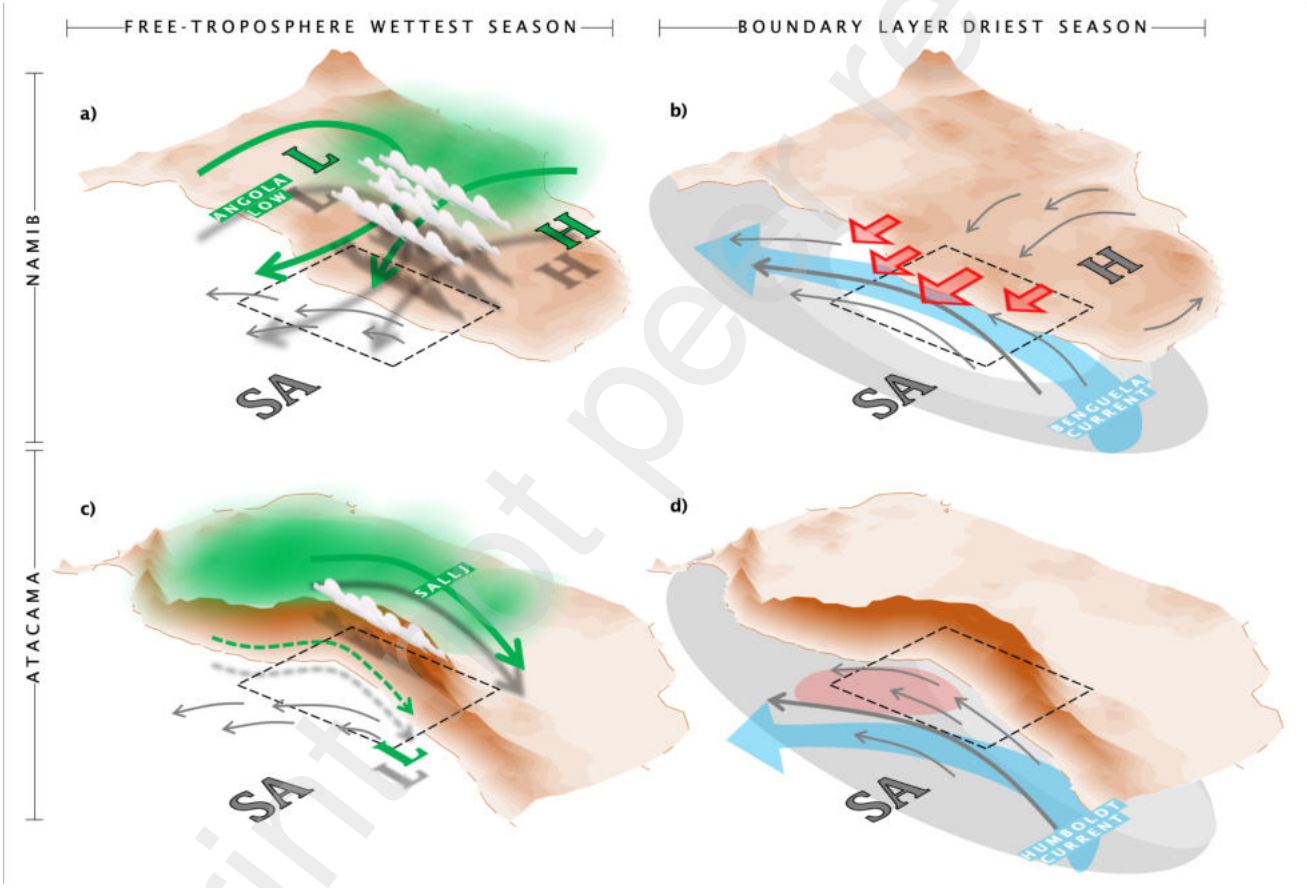

Highlights

A comparative study of the atmospheric water vapor in the Atacama and Namib Desert

Jose Vicencio Veloso, Christoph Böhm, Jan H. Schween, Ulrich Löhnert, and Susanne Crewell

- Free troposphere (FT) humidity contributes between 55-75% of the total column humidity.
- SST control of boundary layer (BL) humidity is higher in the Namib than on the Atacama's coast.
- Frequent continental air mass disrupts the Namib and impacts humidity, drying out the MBL but moistening the FT.
- Similar bordering conditions allow us to extrapolate present-climate moisture variability in the Namib to a paleo-Atacama desert.
- FT moisture transport is observed in Atacama along the coast, potentially increasing humidity in Atacama's hyperarid core.

A comparative study of the atmospheric water vapor in the Atacama and Namib Desert

Jose Vicencio Veloso, Christoph Böhm, Jan H. Schween, Ulrich Löhnert, and Susanne Crewell

[a]*Institute of Geophysics and Meteorology (IGM), University of Cologne, Pohligstrasse 3, Cologne, 50969, North Rhine-Westphalia, Germany*

Abstract

The importance of water vapor in arid and hyperarid regions motivates a comparative study in the Atacama and Namib deserts, a natural laboratory to test the role of topography in present day climate. Based on ERA5 reanalysis evaluated by satellite and ground-based instruments, we focus on the climatological water vapor seasonal cycle offshore the deserts by distinguishing the free-troposphere (FT) and marine boundary layer (MBL) humidity. We found that the sea surface temperature (SST) drives the MBL water vapor seasonal variability in both oceanic regions. However, its effect is less marked in the Namib than in the Atacama. Between fall and winter, easterly continental warm and cloud-free air mass settles over the Namib's coast, reducing the MBL height to a hundred of meters. Additionally, the coastal MBL warms up more than the Benguela current SST, reducing vertical motions, inducing clear-sky conditions and further drying the MBL. On the contrary, year round southerly winds in Atacama's MBL transport cold air over warmer waters due to the Benguela current early turn to the west. This vertical temperature gradient induces a strong coupling between the SST and the MBL humidity, enhanced by a permanent stratocumulus cloud cover. Seasonal differences are also found in the FT. The Namib experiences wetter conditions in summer and spring thanks to moist easterlies and northerlies, respectively. This contrasts with the Atacama where the moisture transport is weaker, maintaining a drier FT year round. We hypothesize that the differences in the humidity seasonality and its controlling mechanisms are strongly associated with differences in topography and the resulting circulation patterns. Furthermore, similar moisture transport and variability could have been part of a paleo-Atacama when its topography

resembled the nowadays Namib Desert.

Keywords: Water vapor, Reanalysis, Atacama, Namib, Free troposphere, Boundary layer

1. Introduction

The Atacama and Namib deserts are considered to be the oldest deserts and two of the driest places on Earth (Houston and Hartley, 2003; Weischet, 1975; Eckardt et al., 2013; Ward et al., 1983). Despite the virtual absence of liquid water and exposure to high UV radiation (e.g. in the Atacama Desert, Rondanelli et al., 2015), microbial life (e.g. Fuentes et al., 2022) and traces of humidity related surface alterations have been found (e.g. Walk et al., 2022) even under such life-threatening conditions. These environments allow the study of life and surface evolution and potential relationships under extreme water limitation (Dunai et al., 2020). For a more profound understanding of such processes, a perspective on the atmospheric water supply that sustains these ecosystems is essential.

The Atacama and Namib Desert are characterized by very similar boundary conditions, responsible for arid (<50mm/year) and hyperarid climate (<5mm/year). As west coast deserts placed within the subtropical high pressure belt, both are affected by near-surface subtropical anticyclones which drive southerly winds along the coast resulting in cold ocean currents (i.e. Humboldt and Benguela for Atacama and Namib, respectively) and upwelling of cold deep waters. The resulting cold and moist marine boundary layer (MBL) is contrasted by large-scale subsidence of warm and dry air (Rodwell and Hoskins, 2001) which leads to the formation of a strong temperature inversion. This inversion hinders vertical air mass exchange so that moisture from the MBL cannot reach the free troposphere. Atmospheric stability is reinforced by stratocumulus cloud formations that cap the MBL (Wang et al., 2004; Wood, 2012).

The prevailing large-scale subsidence inhibits formation of convective clouds, resulting in extremely low precipitation rates (Atacama: 5 mm/year, Houston, 2006; Namib: 20 mm/yr, Southgate et al., 1996). Despite similar boundary conditions, these rates differ by one order of magnitude. This difference implies impacts on the spatio-temporal distribution and rates of geological and biological processes in both deserts. However, no comparative study to identify desert-specific water supply mechanisms exists to date. Fur-

thermore, some authors state that the uplift of the Andes is one of the causes for the extreme dry conditions in the Atacama, by enhancing the rainshadow effect by preventing humidity from the center of the continent to reaching the Atacama (Houston and Hartley, 2003). However, this is still a matter of controversy. First, there is no agreement on the onset of hyperaridity, with evidence suggesting from ∼25 Ma (Dunai et al., 2005) to 1.5 Ma ago (Reich et al., 2009). Second, climate simulations show contradictory results in precipitation changes when topography is reduced in the Atacama Desert (Sepulchre et al., 2009; Ehlers and Poulsen, 2009; Garreaud et al., 2010). A comparative study between the Namib and the Atacama could provide insights on how the transition from arid to hyperarid climate was, considering that the present topography of the Namib Desert resembles a former state of the Atacama Desert when the Andes mountain range were not as high as nowadays, potentially inducing similar weather patterns.

Although the importance of the water vapor as a source of clouds and precipitation has been widely established, its variability across different time scales has not been entirely understood in these regions. For the Atacama Desert, Böhm et al. (2020) show that moister conditions are associated with warmer local sea surface temperature (SST), as well as to the positive phase of El Niño-Southern Oscillation (ENSO) and the Pacific-Decadal Oscillation (PDO). At the same time, the negative phase of the ENSO (La Niña) is linked with both extreme humid and dry conditions in the interanual scale. This contrasting result could be due to the different mechanisms influencing water vapor variability. While La Niña cools the MBL and decreases its humidity, the upper-level Bolivian High intensifies easterly winds, carrying moisture from the center of the continent (Garreaud et al., 2003; Vuille et al., 2003; Farías et al., 2005), and consequently, increasing the water vapor over the desert. This mechanism has been identified as the main source of water vapor for summer precipitation in the Altiplano (>3,500 m ASL, Fig. 1a), located at the east of Atacama and as part of the South American Monsoon (Zhou and Lau, 1998; Vera et al., 2006b). In the Namib, summer precipitation is seemingly more common than in the Atacama, which has been associated with the smoother and more gentle topography (Houston and Hartley, 2003). Some of the most extreme precipitation events in the Namib are triggered by the Angola low and the advection of humidity from the interior of the continent, generating convective storms (Tyson and Preston-Whyte, 2000). In winter, the mechanisms associated with precipitation in both deserts are related to large-scale synoptic features such as cold fronts and cut-off lows

(Tyson and Preston-Whyte, 2000). Water vapor arriving the Atacama is mainly transported in the free-troposphere (FT) long distances often via moisture conveyor belts (MCBs), accounting to >40% of the climatological annual precipitation (Böhm et al., 2021).

One of the major characteristics of the MBL offshore the Namib and the Atacama is the presence of a well established and semi-permanent stratocumulus deck. Within the coastal regions of the deserts, these clouds constitute the most reliable and permanent source of liquid water for the survival of endemic plant species (e.g. Pinto and Kirberg, 2005; Cereceda et al., 2008). Furthermore, these clouds are an important factor in the regulation of Earth's surface temperature due to the high albedo (30-40%), implying a net cooling of the MBL and the surface (Randall et al., 1984; Norris, 1998). Despite the similar bordering conditions, the stratocumulus cloud cover is markedly higher across the Southeast Pacific compared to the Southeast Atlantic according to ship-based (Hanson, 1991) and satellite-based (Stubenrauch et al., 2010) observations. These clouds can reach as far as 100 km inland in the Namib (Olivier, 1995), whereas in the Atacama the coastal cliff (∼1 km ASL, see Fig. 1c) limits inland penetration to the first kilometers from the coast, enhancing the dryness of the inland region (Cereceda et al., 2008). In our study, we aim to identify distinct climatological circulation patterns which could be responsible for these different low cloud patterns.

We suspect that the more gentle and smoothed topography in the Namib Desert allows a more frequent exchange of air masses and moisture between the interior of the continent and the oceanic region compared to the Atacama Desert, that drives a distinct seasonal variability of water vapor and results in different dynamics in the marine boundary layer ultimately affecting cloud, fog, and precipitation patterns. To probe this hypothesis, we investigate and compare the seasonal water vapor variability for the Atacama and the Namib deserts and identify related circulation patterns within the recent climate. Therefore, we focus on integrated water vapor. For a more detailed view on the mechanisms, we distinguish between total water content, water vapor contained in the MBL and in the FT.

To overcome the scarcity of surface-based observations of humidity, as well as upper-air measurements, we apply reanalysis data, which provides the best estimate of the state of the atmosphere based on observations and model physics on a spatial grid. For comparison and validation, we further include satellite and ground-based observations of integrated water vapor.

The paper is structured as follows. In Section 2, we present data and

methods. In Section 3, we evaluate the water vapor from reanalysis by comparing it with satellite and ground-based instruments. The comparison of the integrated water vapor annual mean patterns and seasonal cycles between the Atacama and the Namib is presented in Section 4. In Section 5, we discussed the role of different drivers to explain the differences in water vapor seasonality, separating the analysis in the MBL and FT. We also discussed the effects on clouds, rainfall and moisture variability. Additionally, we discussed how the present climate of the Namib Desert could resemble the paleo-climate of the Atacama Desert. Conclusions are presented in section 6.

2. Data and methods

2.1. Reanalysis

We apply data from the ERA5 reanalysis (Hersbach et al., 2020) with a horizontal resolution of 0.25x0.25 ° latitude-by-longitude for the period 1988–2020 for which a comparison with satellite product is possible. If not explicitly indicated, monthly averages were downloaded from Climate Data Store (CDS). On single and surface level, we use integrated water vapor W_T, sea surface temperature (SST), boundary layer height (BLH), horizontal and vertical winds, as well as low cloud cover (LCC). LCC represents the fraction of a grid box covered by low clouds ($\sim$<2 km AGL). From the ERA5 pressure level data (37 levels) we use specific humidity (q), specific cloud liquid water content, specific rain liquid water content, horizontal winds, vertical velocity (w) and geopotential height. Air temperature (T) and humidity (q) were also obtained from ERA5 model level data set (137 levels). We computed the potential temperature as $\theta = T(P_0/P)^k$, with k the Poison constant ($\sim$ 2/7), P_0 as the surface pressure and P as the pressure at each model level, respectively.

To assess the amount of water vapor contained in the boundary layer and in the free troposphere, we integrated the humidity separately for these two layers. For this purpose, we applied ERA5 q on model level as well surface pressure (SP) and BLH. For each monthly time step, we integrated the q from the surface to the boundary layer top, obtaining the boundary layer water vapor (W_{BL}, Equation 1). For the free-troposphere water vapor (W_{FT}), the integration is performed from the boundary layer top to 150 hPa (Equation 2).

$$W_{BL} = \frac{1}{g} \int_{SP}^{BLH} q dp \tag{1}$$

$$W_{FT} = \frac{1}{g} \int_{BLH}^{150hPa} q dp \tag{2}$$

The amount of vertical grid points for each layer will vary according to the location of the BLH and the 150 hPa level. ERA5 reanalysis defines the BLH using the bulk Richardson number, the most appropriate method according to the conclusions of Seidel et al. (2012). Guo et al. (2021) compared several reanalyses available nowadays, finding that most datasets underestimate the BLH. However, their results indicate that ERA5 exhibits the lowest underestimation (on average 160∼m) of the BLH when compared with daytime radiosondes.

Further, we computed the integrated water vapor transport (IVT, Equation 3; e.g. Ralph et al., 2017).

$$\mathbf{IVT} = \frac{1}{g} \int_{p1}^{p2} q \mathbf{V} \mathrm{d}p \tag{3}$$

where g is the gravity acceleration (-9.8 m/s^2), $\mathbf{V}$ is the horizontal wind vector determined by its meridional and zonal wind components and dp is the difference between pressure levels *p1* and *p2*. These levels are defined later in the text for specific parts of the troposphere.

2.2. Satellite

W_T is investigated using the Remote Sensing System (REMSS) Monthly Mean Total Precipitable Water (Mears et al., 2018). This dataset is a merger of W_T from several passive microwave geophysical ocean products, with 1-degree horizontal resolution and 1-month temporal resolution for the period between 1988–2020. It is available only over ocean excluding near-coastal pixels for which the surface signal cannot be separated properly from the water vapor signal. REMSS W_T is based on data from the following satellite radiometers: SSM/I F08 to F15 (Goodberlet et al., 1989), SSMIS F16 and F17 (Bommarito, 1993), AMSR-E (Kawanishi et al., 2003), WindSat (Gaiser et al., 2004), and AMSR2 (Simpson et al., 1996). According to Mears et al. (2018), errors are in the order of ∼1 kg m^{-2} when compared with soundings and Global Navigation Satellite System (GNSS).

2.3. Ground-based instrumentation

A one-year observations campaign at Iquique Airport (20.54°S, 70.18°W, Fig. 1a) is used to obtain detailed information of W_T at the coast of the Atacama Desert from March 23, 2018, until March 6, 2019 (Schween et al., 2022a). The instrument is a microwave radiometer (MWR) FOGHAT, a 14-channel Humidity and Temperature Profiler (HATPRO, Rose et al., 2005). It performed high-frequency measurements (1 s) of thermal radiation and brightness temperatures in the microwave range, from which W_T is derived (more details can be found in Schween et al., 2022b). We converted the high-frequency data for days with less than 20% of missing data, resulting in 272 days (of a total of 348 days of campaign).

2.4. Study area

We focus on two areas which we term Atacama Oceanic Region and Namib Oceanic Region, indicated in Fig. 1. These areas range between 18-28°S. The longitudes defining the western and eastern margins of the areas change with latitude, following the shape of the shoreline in a distance of about 0.25 degree and keeping a width of 2.75 degrees. These areas represent approximately 310,000 km^2. We restrict these areas to the ocean to avoid the effects of topography and the strong height dependence of W_T. In addition, this procedure enables us to compare the reanalysis with REMSS, a satellite product only available over open ocean.

3. Evaluation of ERA5 IWV from Ground-based instrument and Satellite

We assess the suitability of ERA5 for studying W_T by comparing with REMMS. As our study is based on monthly means, error estimation is based on monthly values from 1988 to 2020. The bias (ERA5 W_T minus REMSS W_T) is -1.31 kg m^{-2} for the Atacama Oceanic Region and -1.42 kg m^{-2} for the Namib Oceanic Region (Fig. 2a), with a bias-corrected (RMSE) of 1.46 kg m^{-2} and 1.52 kg m^{-2}, respectively. Therefore, bias and RMSE are in the order of the uncertainty of REMSS.

The coefficient of determination between ERA5 and REMSS monthly values is high in both oceanic regions, with R^2 of 0.98 for the Atacama and 0.99 for the Namib (Fig. 2a). The linear regression shows an offset of -0.98 kg m^{-2} in the Namib. In the Atacama, the regression indicates a smaller offset (-0.04 kg m^{-2}), evidencing a better agreement for lower monthly values of

W_T. It should be noticed that ERA5 is not totally independent of REMSS. Brightness temperature from six satellite radiometers, including two also used by REMSS (SSM/I and SSMIS), are assimilated into the reanalysis.

Completely independent W_T retrievals are available from the observation campaign at Iquique Airport for the Atacama Desert (Fig. 1a). A comparison between W_T from the MWR and W_T from the nearest ERA5 grid point (Fig. 2b) yields a high linear agreement (R^2=0.95), a slight wet bias in ERA5 of 1.86 kg m^{-2} and a RMSE of 3.34 kg m^{-2}. The overestimation of W_T is observed mainly in the lower values of the distribution.

The high correlation between monthly means of ERA5 and REMSS indicates a good estimation of the seasonal variability of W_T, although an underestimation is present in both oceanic regions. The observed errors are not unusual and are present in other regions of the world with similar differences between independent observations (Steinke et al., 2019). Comparing daily means from the 1-year campaign in the Atacama shows slightly higher RMSE but with a strong correlation, thus indicating a good agreement in the intraseasonal variability of the time series even at the spatial scale of an individual ERA5 grid box. However, it is beyond the scope of this work to determine the origin of the differences.

4. Results

4.1. Annual mean

The overall patterns of the annual average W_T are similar for the Atacama and the Namib, and for both ERA5 and REMSS (Fig. 3). W_T exhibits a marked meridional gradient along the coast, reaching 24 kg m^{-2} around 18°S and decreasing to 15 kg m^{-2} at 28°S. Offshore both deserts, the zonal gradient of W_T is positive over the ocean with the highest values close to the coast in ERA5 (Fig. 3a,c), corroborated by REMSS (Fig. 3b,d). In both deserts, the lowest W_T are found inland. For the Atacama, W_T values range between 0–5 kg m^{-2} (Fig. 3a) in the Altiplano, in agreement with in-situ measurements (Giovanelli et al., 2001). For the Namib Desert, the lowest W_T are about 10 kg m^{-2} (Fig. 3c), which is not as dry as the Atacama mainly due to the lower terrain elevations.

Considering the box offshore both deserts, the climatological annual average of the Atacama Oceanic Region is 16.0 kg m^{-2} according to ERA5, 13% less than for the corresponding region offshore the Namib (18.4 kg m^{-2}, Table 1). This difference is also observed for REMSS, for which W_T averages

17.0 kg m^{-2} for the Atacama Oceanic Region and 19.6 kg m^{-2} for the Namib Oceanic Region (Table 1).

Table 1: Climatological average (1988-2020) of W_T from REMSS, and W_T, W_{FT} and W_{BL} from ERA5, in kg m^{-2}, and the proportion of W_{FT} with respect to W_T for the Atacama Oceanic Region and the Namib Oceanic Region (Fig. 1a and b).

		W_T ERA5	W_T REMSS	W_{BL} ERA5	W_{FT} ERA5	100xW_{FT}/W_T
Atacama	Annual	16.0	17.0	6.3	9.6	60%
	JFM	21.9	23.3	7.9	14.0	64%
	MJJ	13.8	14.7	5.6	8.2	59%
	JJA	12.6	13.4	5.2	7.4	59%
	JAS	12.0	12.8	5.0	7.0	58%
	SON	12.7	13.6	5.5	7.2	57%
Namib	Annual	18.4	19.6	5.2	13.2	72%
	JFM	26.3	27.4	6.7	19.6	75%
	MJJ	13.4	14.6	4.0	9.4	70%
	JJA	12.0	13.1	4.0	8.0	67%
	JAS	12.7	13.7	4.2	8.5	67%
	SON	16.3	17.5	5.0	11.2	69%

For W_{BL}, an inverse zonal gradient compared to W_T is observed over the ocean decreasing from the west towards the coast in both oceanic regions (Fig. 3f,h). The driest conditions with averages of W_{BL} below 5 kg m^{-2} are found in the interior of the Atacama Desert (Fig. 3f). In the case of the Namib, the driest areas in terms of W_{BL} are observed along the coastline (especially around 22–26°S). From the coast to the east, the boundary layer becomes wetter (Fig. 3h). The mean annual W_{BL} in the Atacama Oceanic Region reaches 6.3 kg m^{-2} wetter than the Namib Oceanic Region that averages 5.2 kg m^{-2} (Table 1).

The W_{FT} spatial pattern is more similar to W_T with the highest values near the coast and increasing from south to north for both deserts (Fig. 3f,h). The free-troposphere contributes more to W_{FT} in both oceanic regions, averaging 60% in the Atacama and 72% in the Namib. Furthermore, the Atacama Oceanic Region is 27% drier than the same area offshore the Namib, with an average W_{FT} of about 9.6 and 13.2 kg m^{-2}, respectively (Table 1).

The fact that the spatial pattern of W_{BL} differs from W_{FT} is an indicator that different mechanisms are playing a role in the spatial distribution. Furthermore, from this analysis, it is evident that the yearly average of water vapor is mainly controlled by the free troposphere humidity.

4.2. Water vapor seasonal cycle

For the Atacama and Namib Oceanic Region, monthly mean values of W_T show marked seasonal cycles with amplitudes (difference between annual maximum and minimum) of $\sim$12 kg m^{-2} and $\sim$16 kg m^{-2}, respectively. This is found similarly for both ERA5 and REMSS data (Fig. 4a,b). The moistest season is observed for both deserts within the January-February-March period (JFM), with the Namib being $\sim$17% more humid than the Atacama, reaching between 26.3-27.4 kg m^{-2} and 21.9-23.3 kg m^{-2}, respectively (Table 1). The driest season has similar values of W_T for both deserts (12.0-13.1 kg m^{-2}) observed within the July-August-September period (JAS) in the Atacama Oceanic Region and within the June-July-August period (JJA) in the Namib Oceanic Region.

During the moistest season, the FT in the Namib Oceanic Region is 29% moister than its counterpart region offshore Atacama. Towards the winter, the FT dries out in both deserts, reaching similar values, i.e. the Namib's FT is only 12% wetter than the Atacama's in JJA. However, the Atacama's FT stays relatively dry until November (Fig. 4a), while the Namib experiences a rapid increase in humidity beginning in September (Fig. 4b). The proportion of W_{FT} to W_T is higher in the Namib than in the Atacama, ranging between 64-77% and 55-65%, respectively (Fig. 4). This suggests that most of the W_T seasonal cycle is controlled by the FT humidity, especially in the Namib and in summer in both deserts.

In the MBL, the maximum of W_{BL} is observed for JFM, with an average of 6.3 kg m^{-2} in the Atacama Oceanic Region and 5.2 kg m^{-2} in the Namib Oceanic Region (Table 1). After the summer, the Namib dries out faster than the Atacama, reaching a minimum of 4.0 kg m^{-2} within the May-June-July season (MJJ) and 5.0 kg m^{-2} in Atacama in July-August-September (JAS) period (Fig. 4). In the following section, we discuss the drivers of the humidity seasonal variability for the boundary layer and the free-troposphere.

5. Discussion

5.1. Marine boundary layer

The seasonality of W_{BL} can be linked to the interaction with several factors, such as SST, BLH, stratocumulus feedback and winds. The SST modulates temperature and humidity of the MBL through heat and moisture fluxes at the ocean-atmosphere interface. In the Atacama Oceanic Region, W_{BL} varies seasonally in phase with the SST, with their maximum and minimum values occurring at the same time (Fig. 4c). The monthly values of SST and W_{BL} show a coefficient of determination (R^2) of 0.81 (Fig. 5a). In the Namib Oceanic Region, the SST experiences a similar seasonal cycle compared to its counterpart in the Atacama (Fig. 4d). However, only the summer maxima of SST and W_{BL} coincide in respect of their timing. The driest MBL of the Namib Oceanic Region occurs already early in the season (MJJ) whereas the SST reaches its minimum two months later (JAS). This seasonal offset is manifested in a lower correlation between SST and W_{BL} ($R^2 \approx 0.45$) compared to the Atacama (Fig. 5b). This points that the MBL water vapor content offshore the Namib Desert seems to be partially decoupled from the SST and driven by other factors during fall/winter.

To further explain the weaker correlation, we investigated the role of the MBL thickness and low clouds. Offshore the Namib, the seasonal cycle of the BLH (Fig. 6a) agrees with the W_{BL}, with the thinnest MBL observed between April-July. The evolution of the mean BLH hides a wide interdaily variability, with some days having BLH reaching up to 1200 m ASL and others close to 100 m ASL (Fig. 6a). The distribution is skewed towards lower values of BLH (<400 m ASL), an indication that the otherwise typical subtropical MBL is replaced by a shallow boundary layer. Moreover, the LCC offshore the Namib (Fig. 6b) denotes a marked reduction during the shallower BLH period, with a daily distribution skewed toward lower values and cloud free conditions dominating in this period. In contrast, the Atacama Oceanic Region rarely observes clear-sky conditions and the LCC is more than double than in the Namib year round (Fig. 6b). Furthermore, the LCC and the BLH show smaller seasonal variations in the Atacama than in the Namib. Due to the key role of the stratocumulus clouds to maintain coupling with its surface moisture supply through turbulence (Wood, 2012), we investigate the stability of the BL derived from the average θ in the MBL (θ_{MBL}), surface (θ_{sf}), top MBL (θ_{MBLtop}), and lower FT (θ_{900hPa}, Fig. 7)

The Atacama Oceanic Region MBL is colder than the SST year round, with a $\delta\theta$ of $\sim$-1.4 K (θ_{MBL} minus SST). A colder air mass over warmer SST induces the rise of surface air parcels and triggers cloud formation, efficiently mixing the MBL as can be observed in the vertical profiles of q for the main seasons analyzed (Fig. 8) and the small gradient between θ_{sf} and θ_{MBLtop}. Contrary to the Atacama, the mean MBL θ offshore the Namib is warmer than the SST (Fig. 7b). The difference ranges from 0.5 K in January to 2.4 K in July, suggesting the presence of an on averaged-stable layer where the MBL is constrained to just a few hundred of meters. This feature is particularly notorious between April-July, driven by two factors. While the surface θ cools due to the SST cooling from summer to winter, the top of the MBL and the lower FT (900 hPa) warms up (Fig. 7b).

A more detailed analysis of the vertical structure of winds, humidity and clouds is presented in a cross-section in Fig 9, averaged from 18-28°S for JAS in the Atacama and MJJ in the Namib (Fig. 9). In the Namib, easterly winds cross from surface to 800 hPa from the interior of the continent. The observed MBL warming is caused by these enhanced easterly winds that transport drier and cloud-free continental air from the interior of the desert to the oceanic region. Additionally, these winds develop a descending component while crossing the Namib Desert, further warming and drying the air mass. In the Atacama, easterly winds are also present in most of the MBL and low FT, although they are much weaker than in the Namib. Furthermore, the winds close to the coast and near the surface present a westerly direction, which seems to enhance the humidity along the coast by air mass convergence. The cloud pattern offshore both deserts is also remarkably different. The Atacama observes an in average well-developed MBL with high cloud liquid water content and precipitation (drizzle) as expected in the stratocumulus clouds in this region (see Schween et al., 2022b). In the Namib, stratocumulus cloud cover is still present, but with lower cloud liquid water content and a shallower cloud base height.

We suspect that the easterly winds are synoptic-driven events lasting from hours to a couple of days, creating a marked dry and warm layer capping a shallow MBL, followed by days with a more developed and well-mixed MBL. In MJJ, the winds inland at 850 hPa (Fig. 10b) show a clear anticyclonic circulation, which in combination with lower pressures along the coast, leads to easterly winds crossing from inland to the open ocean. The stratocumulus cloud cover reduction interrupts the mixing in the MBL, decoupling it from the surface moisture source. Therefore, Namib's W_{BL} is partially controlled

by the SST, but also by the LCC. The R^2 between W_{BL} and LCC is 0.44 (Fig. 5b), as high as with the SST, explaining why low W_{BL} values occur over a wider range of SST in comparison with the Atacama Oceanic Region. In spring (SON), MBL southerly winds resume circulation along the coast (Fig. 10f), inducing the BLH and LCC recovery, as well an increment in W_{BL}. The stratocumulus driven mixing in the MBL reappears thanks to the less frequent continental air disruption, permitting the humidity to increase especially in the middle and upper MBL (Fig. 8d), despite that the cooling of the SST towards the spring.

We propose that the observed differences in W_{BL}, LCC and BLH seasonality are related to the topography. The presence of the Andes mountains (>4 km ASL) reduces the probability of air mass exchange within the MBL between the interior of the continent and the coast, maintaining MBL winds parallel to the shoreline and without any noticeable influence of continental air (Fig. 10a,c,e). This allows the development of an unperturbed MBL throughout the year, expressed in a less marked BLH and LCC seasonal cycle in comparison to the Namib, as well a marked stratocumulus cover during the MBL driest period. The constant southerly winds transport cold air over progressively warmer waters because the Humboldt Current leaves the Atacama's coast around 24°S, which allows warmer water to move southward (Fig. 11a, Schween et al. (2022b)). The SST/air temperature gradient enhances vertical motions, inducing a stratocumulus cloud cover almost permanent throughout the year. Observational studies and simulations with numerical models seem to confirm the presence of a well mixed marine boundary layer offshore Atacama (Serpetzoglou et al., 2008; Muñoz et al., 2011; del Río et al., 2021; Schween et al., 2022b), allowing us to have confidence in the observed MBL structure from ERA5. In the Namib Oceanic Region, the smoothed topography is conducive to the disruption of the coastal MBL by inland air masses triggered by regional synoptic patterns. The continental warm/dry air from the east induces a less strong SST control of the W_{BL} by reducing the cloud cover, the mixing and the MBL height. Additionally, the drier MBL offshore the Namib is also linked to the Benguela current, which stays further north close the coast than the Humboldt current (Fig. 11b).

The results of our comparative study are in line with previous works. For instance, Xu et al. (2004) used a regional atmospheric model to test the effect of the South American topography on the regional climate. They found that the stratocumulus offshore Peru (10-20°S) are reduced if the Andes are completely removed, due to the advection of warm air from the east within

the BL. Similar to this, Richter and Mechoso (2004) used an atmospheric general circulation model to reduce the topography of the Namib to zero, finding that the cloud cover offshore Angola (10-20°S) and Namibia also experiences a reduction. The authors discuss that nowadays Namib topography enhanced static stability in the lower troposphere (700 hPa) as a result of warm advection in the lower FT and cold southerly winds near the surface. These mechanisms are weakened if the topography is reduced, in agreement with our comparative study between the Atacama and the Namib.

5.2. Free troposphere

During the moistest season (JFM) the FT of the Namib Oceanic Region is much wetter (W_{FT} = 20.8 kg m^{-2}) than its counterpart at the Atacama (W_{FT} = 14.7 kg m^{-2}) due to a humidity excess at height levels between 850-500 hPa for which q differs by a factor of two (Fig. 8a). This is the result of marked moist easterly winds between the surface and 500 hPa crossing the coast from the interior of the continent to the open ocean (Fig. 12b). The moisture intrusion is particularly pronounced between 825-700 hPa. In this layer, a strong IVT corridor results from the interaction of the Angola Low and the northeast of Namib (Tyson and Preston-Whyte, 2000) and the continental high pressure in the southeastern region of South Africa (H in Fig. 13b). The mostly meridional geopotential gradient between these two systems results in mostly westward-oriented IVT ranging between 5 kg m s^{-1} in the southern part (∼24°S) of the Namib and 25 kg m s^{-1} in the northern part (∼18°S). For the Atacama, ERA5 reanalysis shows southward moisture transport at the east of the Andes in association with the South American Low-Level Jet (SALLJ, as described, for example, in Vera et al., 2006a), with no relevant moisture transfer into the desert (Fig. 13a). The vertical cross-section over the Atacama shows, climatologically, an opposite circulation compared to the Namib, with westerly winds predominating in most of the troposphere during the summer (Fig. 12a).

The FT of both deserts dries out toward the winter, reaching a minimum in JJA in the Namib and in JAS in the Atacama. However, the former observes a rapid increase in the humidity during SON, while the Atacama continues to be dry until November (Fig. 4a). Both deserts experience similar drying of the lower FT (925-800 hPa) from JJA to SON (Fig. 8d), associated with the period of the strongest subsidence (Fig. 4c,d) and the maximum intensity of the subtropical anticyclones around spring (Mächel et al., 1998; Ancapichún and Garcés-Vargas, 2015). However, for the Namib

increased q between 800-500 hPa (Fig. 8c,d) is due to the establishment of a high pressure system over South Africa, enhancing moisture transport from the tropics (Fig. 13f). The moisture transport overcompensates the drying of the Namib's lower FT. The drier Atacama's FT in comparison with the Namib is due to the absence of any moisture transport during spring (Fig. 13e), so that the intensification of the anticyclone dries the atmosphere.

5.3. Summer clouds, rainfall, and moisture intrusion

The moistest season in the Namib Oceanic Region is characterized by enhanced cloud development mainly at the east of the desert (Fig. 12d) in connection to the strong summer convection in the interior of the continent and the Intertropical Convergence Zone (ITCZ, Suzuki, 2011). ERA5 also estimates precipitation below these high-based clouds, mostly inland and decreasing in magnitude as we get closer to the coast. Precipitation records in the core of the Namib reveal that most rainfall episodes are associated with the Angola Low and the advection of humidity from the east (Eckardt et al., 2013). Additionally, the specific rain water content below this high-based clouds decreases towards the surface, suggesting evaporation in the lower part of the troposphere (Fig. 12d). This phenomenon, named virga, has been identified in the Namib Desert by satellite observations to account for between 30-50% of the total precipitation events (Wang et al., 2018), which agrees with the estimated reduction of the specific rain liquid water from ERA5 between 650 hPa and the surface. This addition of water vapor could also explain the moister conditions in the Namib's interior, as well as a potential source for radiative fog in the area.

The Atacama's FT is not affected by major humidity transport compared to the Namib, except for a weak IVT structure present in the lower free-troposphere between 10-22°S offshore Peru and Northern Chile (Fig. 13a). The origin of this transport is related to a positive meridional pressure gradient along the coast with lower geopotential height to the south of the Atacama and a closed low-pressure system between 825-875 hPa that has not been identified or described in previous studies (Fig. 13c). The northerly winds are evident in the vertical cross-section (Fig. 12a) with a maximum of -1 m/s at 850 hPa and accompanied by enhanced humidity above the MBL. It seems plausible that these northerlies are efficiently providing humidity to the interior of Atacama. The near surface circulation pattern from ERA5, both daily average (Fig. 12a) and daytime average (not shown), shows a west-to-east circulation, in agreement with the expected diurnal pattern for

summer due to the warming of the western slope of the Andes, i.e. the Rutllant cell (Rutllant et al., 2003). According to ERA5 winds transport the humidity towards the east, triggering clouds, fog, and precipitation in the eastern margin of the Atacama (i.e., the precordillera, ∼69°W, Fig. 12c).

The fact that the IVT structure appears as a weak signal in the climatology may be an indicator that this is a rare synoptic feature rather than a stable climatic pattern. Using ERA5 reanalysis, Vicencio (2021) found that an extreme rainfall event during January 2020 was triggered by an atmospheric river like structure along the coast of Peru and Chile, resembling the climatological IVT pattern presented in this study. Because the humidity reaches the coast above the MBL and the coastal cliff, the Rutllant cell easily transports this humidity inland, triggering convection and rain across the Atacama but especially in the precordillera. Furthermore, Reyers et al. (2021) performed high-resolution simulations of the present climate of the Atacama using WRF, finding a cluster of rainfall episodes affecting mainly the precordillera in association with moist air coming from the west. Up to now, knowledge on summer precipitation in the Atacama is limited and most of the research has been focused on the Altiplano, a region impacted by frequent storms during the summer due to the transport of humidity from the center of the continent (Garreaud et al., 2003; Vuille et al., 2003; Farías et al., 2005). Our results demonstrate that moisture originated in the Pacific could also be a source for precipitation in the Atacama, and it should be taken to account for future works.

5.4. The past of the Atacama, the present of the Namib

We showed that nowadays circulation patterns in the Atacama and the Namib region trigger contrasting humidity transport mechanisms, which ultimately control the moisture availability in over the desert and offshore. The major difference between both arid regions is the topography, understood as both the altitude of the Andes mountain range and its north-to-south extension across South America in comparison with the absence of similar features in South Africa. Therefore, these areas become a natural laboratory to study the sensitivity of weather patterns as a result of the topographic forcing, considering that the current Namib's topography resembles a former Atacama Desert around 25-20 Ma ago when its altitude was 1/4 of nowadays (1000-2000 m ASL, Gregory-Wodzicki, 2000). This hypothesis is plausible considering that other important factors were also present during the late Oligocene, e.g. the nearly fixed position of the South American continent in

the last 150 Ma (Hartley et al., 2005) thus maintaining similar distance to the subtropical anticyclone influence and to the mid-latitude disturbances, and a cold current along the western coast of South America present since at least ∼50 Ma (Marty et al., 1988) due to the opening of the Drake passage and the establishment of the Antarctic Circumpolar Current (Scher and Martin, 2006; Lagabrielle et al., 2009).

The changes in South America's topography and its effects on precipitation have been investigated by using global circulation models. For instance, Sepulchre et al. (2009) and Garreaud et al. (2010) found little to no changes in rainfall rates in the Atacama when topography is reduced to zero (this, a flat continent), concluding that the rise of the Andes has no effect on the hyperaridity onset. However, it is important to note that these models have poor horizontal resolutions (140 and 250 km, respectively), which may not capture differences in subgrid precipitation patterns. Given that the Atacama's west-to-east extent ranges between 100-200 km, these models may not adequately capture the fine-scale variations in precipitation that are relevant to understanding the region's hyperaridity. Additionally, the models do not fully capture the nature of convective precipitation during summer months, reproducing good large-scale patterns but with wrong regional structures (see discussion in Garreaud et al., 2010), which leads to unrealistic results. In contrast, Ehlers and Poulsen (2009) used a regional circulation model with higher horizontal resolution (60 km), finding that reduced topography leads to increased precipitation on the western flank of the Andes, including the Atacama. This increment is associated with marked moisture transport from the east, thanks to the formation of a low-level low-pressure system at the northeast of the Atacama Desert (see Fig. 4d in Ehlers and Poulsen, 2009) similar to the Angola Low described in our study. In present day climate, the moisture transport from the east accounts for the majority of rainfall events between mid-summer and autumn in the Namib (Eckardt et al., 2013) becoming this period in the wettest of year (Eckardt et al., 2013; Lancaster et al., 1984). However, the Atacama lacks precipitation in this period, suggesting that this easterly-sourced rainfall is missing.

We hypothesize that the rise of the Andes cordillera gradually altered the atmospheric circulation pattern, producing a reduction in the amount of humidity advected from the east in summer/autumn and therefore reducing the frequency of storms and rainfall events in agreement with the rainshadow effect proposed by Houston and Hartley (2003). This transition contributed to a shift in the Atacama's climate from mainly arid, similar to present-day

Namib with rainfall amounts between 3-88 mm/year (Seely and Louw, 1980; Lancaster et al., 1984; Southgate et al., 1996), to extended hyperaridity with averages between 0.15-4.1 mm/year (Houston, 2006). While the aridification process reduced precipitation across the Atacama, the effect was not uniform throughout the desert. The driest region was located farthest from the humidity source (i.e., the coast), primarily as a result of the greater distance from the eastward-moving storms and associated moisture, similar to the west-east rainfall pattern in the Namib nowadays. Continued uplift of the Andes cordillera is likely to further intensify the aridification of the desert's interior. This pattern of drying is supported by various studies. The earliest estimates of the Atacama hyperaridity onset (∼25 Ma) considered the absence of major erosion by taking samples next to the coast (i.e., the Coastal Cordillera, Dunai et al., 2005). When studies used evidence in the interior of the desert and the precordillera (supergene mineralization) the onset of the hyperaridity is placed between 19-13 Ma (Rech et al., 2006; Sillitoe and McKee, 1996). Therefore, the range of dates for the onset of hyperaridity may not be necessarily contradictory, but rather complementary by reflecting the gradual progression of aridification, from the coast towards the desert interior. Our hypothesis states that today's climate in the Namib Desert resembles a former Atacama Desert before the Andes uplift. Nevertheless, it must be considered in the discussion that other studies suggest a more recent transition to hyperarid conditions in the Atacama (∼8 to 1.5 Ma), which may indicate other climatic factors playing a role (Hartley and Chong, 2002; Amundson et al., 2012; Reich et al., 2009).

6. Conclusions

We analyzed the W_T seasonal cycle for the contiguous oceanic regions offshore the Atacama and the Namib Desert, using state-of-the-art reanalysis evaluated with satellite retrievals. We studied the seasonal variability of W_T, as well as the driving mechanisms, separating the amount of humidity in the BL and in the FT.

The FT contributes between 55–75 % of the total column humidity, driving the seasonal cycle of W_T. During the moistest season (JFM), the Namib's FT is around 18 % moister than the Atacama due to humidity transport from the interior of the continent controlled by the Angola Low (Fig. 14a). This transport leads to cloud and precipitation formation, which affect mainly the eastern margin of the Namib Desert. In contrast, there is no major climato-

logical transport of humidity in the Atacama and the humidity of the core of the South American continent does not reach the desert. However, we found a weak structure of moisture transport along the coast of Peru and Northern Chile, in a band-like structure in the lower FT (850 hPa, Fig. 14c). This structure has not been identified in previous climatological studies in the area, and it seems relevant as a source of humidity for the Atacama's hyperarid core, as well as a source of clouds and precipitation in the Precordillera and Altiplano (Fig. 14c). The FT dries from summer to winter, reaching the driest trimester in JJA in the Namib and JAS in the Atacama due to the reduction of humidity transport, as well as the intensification of the subsidence of the subtropical anticyclones. After reaching the minimum of humidity, the Namib observes a rapid increase in moisture in spring due to a lower free-troposphere circulation pattern that induces the tipping of humidity from the tropical northeast Atlantic region toward the desert. In contrast, the Atacama Desert does not experience any relevant transport of humidity in the FT, maintaining similar dry conditions until late spring.

The Namib's MBL is about 21% drier than its counterpart in the Atacama, reaching the lowest W_{BL} in MJJ whereas in the Atacama it occurs in JAS. The SST seasonality partially explains the water vapor seasonal cycle offshore the Namib. For instance, the Benguela current is colder than the Humboldt current, reducing the evaporation and the humidity content in the MBL. Additionally, Namib's MBL is warmer than the SST year round. This induces a notable reduction in the well-mixed MBL altitude, constrained to just a few hundred of meters during the April-July period thanks to westward air mass transport. The dry, warm and cloud-free continental air caps the shallow MBL along the coast. By reducing the cloud cover, the stratocumulus driven mixing stops and the coupling with the ocean surface is reduced, inducing a minimum of humidity months before the minimum expected by SST control only (Fig. 14b). In the Atacama Oceanic Region, the seasonal cycle of the W_{BL} is strongly correlated with the SST. The cold air transport from the south in connection with the Humboldt current gyre favors a well mixed MBL. Additionally, the stratocumulus deck offshore suffers little seasonal variations compared to the Namib over the year, reinforcing the stratocumulus driven mixing and the coupling with the moisture supply from the ocean (Fig. 14d).

Our comparative study points out the importance of distinguishing between the FT and BL to identify the driving mechanisms of water vapor seasonality. Additionally, we considered both deserts as a natural laboratory

to test the effect of differences in topography on atmospheric circulation patterns, which ultimately affects the humidity transport, rainfall, and clouds. The presence of the Andes mountain range not only seems to block any major moisture exchange between the interior continent and the coast of Atacama, but also prevents exchange between the marine and continental boundary layer. In addition, the smoother topography of the Namib Desert allows the development of different climatological synoptic patterns influencing the water vapor transport, which are not present in the vicinity of the Atacama. This motivates the hypothesis that the current moisture transport mechanisms in the Namib Desert could resemble the patterns in the past climate of the Atacama Desert when the topography of South America was significantly lower and similar to South Africa today. The reduction of the humidity transport from the interior of the continent (the rainshadow effect) induced a transition in the Atacama from arid (such as in the Namib nowadays) to hyperarid conditions as the Andes uplifted due to the reduction of summer and fall east originated precipitation.

References

Amundson, R., Dietrich, W., Bellugi, D., Ewing, S., Nishiizumi, K., Chong, G., Owen, J., Finkel, R., Heimsath, A., Stewart, B., Caffee, M., 2012. Geomorphologic evidence for the late Pliocene onset of hyperaridity in the Atacama Desert. GSA Bulletin 124, 1048–1070. doi:10.1130/B30445.1.

Ancapichún, S., Garcés-Vargas, J., 2015. Variability of the Southeast Pacific Subtropical Anticyclone and its impact on sea surface temperature off north-central Chile. Ciencias Marinas 41, 1–20. doi:10.7773/cm.v41i1.2338.

Bommarito, J.J., 1993. DMSP special sensor microwave imager sounder (SSMIS), in: Microwave Instrumentation for Remote Sensing of the Earth, SPIE. pp. 230–238.

Böhm, C., Reyers, M., Knarr, L., Crewell, S., 2021. The role of moisture conveyor belts for precipitation in the atacama desert. Geophysical Research Letters 48, e2021GL094372. doi:https://doi.org/10.1029/2021GL094372. e2021GL094372 2021GL094372.

Böhm, C., Reyers, M., Schween, J.H., Crewell, S., 2020. Water vapor variability in the atacama desert during the 20th century. Global and Planetary Change 190, 103192. doi:https://doi.org/10.1016/j.gloplacha.2020.103192.

Cereceda, P., Larrain, H., Osses, P., Farías, M., Egaña, I., 2008. The spatial and temporal variability of fog and its relation to fog oases in the Atacama Desert, Chile. Atmospheric Research 87, 312–323. doi:https://doi.org/10.1016/j.atmosres.2007.11.012.

Dunai, T.J., López, G.A.G., Juez-Larré, J., 2005. Oligocene–Miocene age of aridity in the Atacama Desert revealed by exposure dating of erosion-sensitive landforms. Geology 33, 321–324. doi:10.1130/G21184.1.

Dunai, T.J., Melles, M., Quandt, D., Knief, C., Amelung, W., 2020. Whitepaper: Earth – evolution at the dry limit. Global and Planetary Change 193, 103275. doi:https://doi.org/10.1016/j.gloplacha.2020.103275.

Eckardt, F., Soderberg, K., Coop, L., Muller, A., Vickery, K., Grandin, R., Jack, C., Kapalanga, T., Henschel, J., 2013. The nature of moisture at Gobabeb, in the central Namib Desert. Journal of Arid Environments 93, 7–19. doi:https://doi.org/10.1016/j.jaridenv.2012.01.011.

Ehlers, T.A., Poulsen, C.J., 2009. Influence of Andean uplift on climate and paleoaltimetry estimates. Earth and Planetary Science Letters 281, 238–248. doi:https://doi.org/10.1016/j.epsl.2009.02.026.

Farías, M., Cereceda, P., Osses, P., Núñez, R., 2005. Spatial and temporal behavior of the stratocumulus cloud, fog producer in the coast of the Atacama desert (21 south lat., 70 west long.), during one month of winter and another of summer. Investigaciones geográficas , 43–61.

Fuentes, B., Choque, A., Gómez, F., Alarcón, J., Castro-Nallar, E., Arenas, F., Contreras, D., Mörchen, R., Amelung, W., Knief, C., Moradi, G., Klumpp, E., Saavedra, C.P., Prietzel, J., Klysubun, W., Remonsellez, F., Bol, R., 2022. Influence of Physical-Chemical Soil Parameters on Microbiota Composition and Diversity in a Deep Hyperarid core of the Atacama Desert. Frontiers in Microbiology 12. doi:10.3389/fmicb.2021.794743.

Gaiser, P.W., St Germain, K.M., Twarog, E.M., Poe, G.A., Purdy, W., Richardson, D., Grossman, W., Jones, W.L., Spencer, D., Golba, G., et al.,

2004. The WindSat spaceborne polarimetric microwave radiometer: Sensor description and early orbit performance. IEEE Transactions on Geoscience and Remote Sensing 42, 2347–2361.

Garreaud, R., Molina, A., Farias, F., 2010. Andean uplift, ocean cooling and Atacama hyperaridity: A climate modeling perspective. Earth and Planetary Science Letters 292(1-2), 39–50.

Garreaud, R., Vuille, M., Clement, A.C., 2003. The climate of the Altiplano: observed current conditions and mechanisms of past changes. Palaeogeography, palaeoclimatology, palaeoecology 194, 5–22.

Giovanelli, R., Darling, J., Henderson, C., Hoffman, W., Barry, D., Cordes, J., Eikenberry, S., Gull, G., Keller, L., Smith, J.D., Stacey, G., 2001. The Optical/Infrared Astronomical Quality of High Atacama Sites. ii. Infrared Characteristics. Astronomical Society of the Pacific 113, 803–813. doi:10.1086/322136.

Goodberlet, M.A., Swift, C.T., Wilkerson, J.C., 1989. Remote sensing of ocean surface winds with the special sensor microwave/imager. Journal of Geophysical Research: Oceans 94, 14547–14555. doi:https://doi.org/10.1029/JC094iC10p14547.

Gregory-Wodzicki, K.M., 2000. Uplift history of the Central and Northern Andes: A review. GSA Bulletin 112, 1091–1105. doi:10.1130/0016-7606(2000)112¡1091:UHOTCA¿2.0.CO;2.

Guo, J., Zhang, J., Yang, K., Liao, H., Zhang, S., Huang, K., Lv, Y., Shao, J., Yu, T., Tong, B., Li, J., Su, T., Yim, S.H.L., Stoffelen, A., Zhai, P., Xu, X., 2021. Investigation of near-global daytime boundary layer height using high-resolution radiosondes: first results and comparison with ERA5, MERRA-2, JRA-55, and NCEP-2 reanalyses. Atmospheric Chemistry and Physics 21, 17079–17097. doi:10.5194/acp-21-17079-2021.

Hanson, H.P., 1991. Marine stratocumulus climatologies. International Journal of Climatology 11, 147–164. doi:https://doi.org/10.1002/joc.3370110204.

Hartley, A.J., Chong, G., 2002. Late Pliocene age for the Atacama Desert: implications for the desertification of western South America. Geology 30, 43–46.

Hartley, A.J., Chong, G., Houston, J., Mather, A.E., 2005. 150 million years of climatic stability: evidence from the Atacama Desert, northern Chile. Journal of the Geological Society 162, 421–424. doi:10.1144/0016-764904-071.

Hersbach, H., Bell, B., Berrisford, P., Hirahara, S., Horányi, A., Muñoz-Sabater, J., Nicolas, J., Peubey, C., Radu, R., Schepers, D., Simmons, A., Soci, C., Abdalla, S., Abellan, X., Balsamo, G., Bechtold, P., Biavati, G., Bidlot, J., Bonavita, M., De Chiara, G., Dahlgren, P., Dee, D., Diamantakis, M., Dragani, R., Flemming, J., Forbes, R., Fuentes, M., Geer, A., Haimberger, L., Healy, S., Hogan, R.J., Hólm, E., Janisková, M., Keeley, S., Laloyaux, P., Lopez, P., Lupu, C., Radnoti, G., de Rosnay, P., Rozum, I., Vamborg, F., Villaume, S., Thépaut, J.N., 2020. The ERA5 global reanalysis. Quarterly Journal of the Royal Meteorological Society 146, 1999–2049. doi:https://doi.org/10.1002/qj.3803.

Houston, J., 2006. Variability of precipitation in the Atacama Desert: its causes and hydrological impact. International Journal of Climatology 26, 2181–2198. doi:10.1002/joc.1359.

Houston, J., Hartley, A.J., 2003. The central Andean west-slope rainshadow and its potential contribution to the origin of hyper-aridity in the Atacama Desert. International Journal of Climatology 23, 1453–1464. doi:10.1002/joc.938.

Kawanishi, T., Sezai, T., Ito, Y., Imaoka, K., Takeshima, T., Ishido, Y., Shibata, A., Miura, M., Inahata, H., Spencer, R.W., 2003. The Advanced Microwave Scanning Radiometer for the Earth Observing System (AMSR-E), NASDA's contribution to the EOS for global energy and water cycle studies. IEEE Transactions on Geoscience and Remote Sensing 41, 184–194.

Lagabrielle, Y., Goddéris, Y., Donnadieu, Y., Malavieille, J., Suarez, M., 2009. The tectonic history of Drake Passage and its possible impacts on global climate. Earth and Planetary Science Letters 279, 197–211. doi:https://doi.org/10.1016/j.epsl.2008.12.037.

Lancaster, J., Lancaster, N., Seely, M., 1984. Climate of the central Namib Desert. MADOQUA 14, 5–61.

Marty, R., Dunbar, R., Martin, J.B., Baker, P., 1988. Late Eocene diatomite from the Peruvian coastal desert, coastal upwelling in the eastern Pacific, and Pacific circulation before the terminal Eocene event. Geology 16, 818–822. doi:10.1130/0091-7613(1988)016¡0818:LEDFTP¿2.3.CO;2.

Mears, C.A., Smith, D.K., Ricciardulli, L., Wang, J., Huelsing, H., Wentz, F.J., 2018. Construction and Uncertainty Estimation of a Satellite-Derived Total Precipitable Water Data Record over the World's oeans. Earth and Space Science 5, 197–210. doi:https://doi.org/10.1002/2018EA000363.

Muñoz, R.C., Zamora, R.A., Rutllant, J.A., 2011. The Coastal Boundary Layer at the Eastern Margin of the Southeast Pacific (23.4 S, 70.4 W): Cloudiness-Conditioned Climatology. Journal of Climate 24, 1013 – 1033. doi:10.1175/2010JCLI3714.1.

Mächel, H., Kapala, A., Flohn, H., 1998. Behaviour of the centres of action above the Atlantic since 1881. Part I: Characteristics of seasonal and interannual variability. International Journal of Climatology 18, 1–22. doi:https://doi.org/10.1002/(SICI)1097-0088(199801)18:1¡1::AID-JOC225¿3.0.CO;2-A.

Norris, J.R., 1998. Low cloud structure over the ocean from surface observations. Part II: Geographical and seasonal variations. Journal of Climate 11, 383–403. doi:https://doi.org/10.1175/1520-0442(1998)011¡0383:LCTOTO¿2.0.CO;2.

Olivier, J., 1995. Spatial distribution of fog in the Namib. Journal of Arid Environments 29, 129–138. doi:https://doi.org/10.1016/S0140-1963(05)80084-9.

Pinto, R., Kirberg, A., 2005. Conservation status of Eriosyce (Cactaceae) in northernmost Chile. Bradleya 2005, 7–16. doi:10.25223/brad.n23.2005.a3.

Ralph, F.M., Iacobellis, S.F., Neiman, P.J., Cordeira, J.M., Spackman, J.R., Waliser, D.E., Wick, G.A., White, A.B., Fairall, C., 2017. Dropsonde Observations of Total Integrated Water Vapor Transport within North Pacific Atmospheric Rivers. Journal of Hydrometeorology 18, 2577 – 2596. doi:10.1175/JHM-D-17-0036.1.

Randall, D.A., Coakley, J.A., Fairall, C.W., Kropfli, R.A., Lenschow, D.H., 1984. Outlook for Research on Subtropical Marine Stratiform

Clouds. Bulletin of the American Meteorological Society 65, 1290 – 1301. doi:10.1175/1520-0477(1984)065¡1290:OFROSM¿2.0.CO;2.

Rech, J.A., Currie, B.S., Michalski, G., Cowan, A.M., 2006. Neogene climate change and uplift in the Atacama Desert, Chile. Geology 34, 761–764.

Reich, M., Palacios, C., Vargas, G., Luo, S., Cameron, E.M., Leybourne, M.I., Parada, M.A., Zúñiga, A., You, C.F., 2009. Supergene enrichment of copper deposits since the onset of modern hyperaridity in the Atacama Desert, Chile. Mineralium Deposita 44, 497–504.

Reyers, M., Böhm, C., Knarr, L., Shao, Y., Crewell, S., 2021. Synoptic-to-regional scale analysis of rainfall in the Atacama Desert (18S–26S) using a long-term simulation with WRF. Monthly Weather Review 149(1), 91–112. doi:https://doi.org/10.1175/MWR-D-20-0038.1.

Richter, I., Mechoso, C.R., 2004. Orographic influences on the annual cycle of Namibian stratocumulus clouds. Geophysical Research Letters 31. doi:https://doi.org/10.1029/2004GL020814.

Rodwell, M.J., Hoskins, B.J., 2001. Subtropical Anticyclones and Summer Monsoons. Journal of Climate 14, 3192 – 3211. doi:10.1175/1520-0442(2001)014¡3192:SAASM¿2.0.CO;2.

Rondanelli, R., Molina, A., Falvey, M., 2015. The Atacama Surface Solar Maximum. Bulletin of the American Meteorological Society 96, 405 – 418. doi:10.1175/BAMS-D-13-00175.1.

Rose, T., Crewell, S., Löhnert, U., Simmer, C., 2005. A network suitable microwave radiometer for operational monitoring of the cloudy atmosphere. Atmospheric Research 75, 183–200. doi:https://doi.org/10.1016/j.atmosres.2004.12.005. cLIWA-NET: Observation and Modelling of Liquid Water Clouds.

Rutllant, J., Fuenzalida, H., Aceituno, P., 2003. Climate dynamics along the arid northern coast of Chile: The 1997–1998 Dinámica del Clima de la Región de Antofagasta (DICLIMA) experiment. Journal of Geophysical Research: Atmospheres 108. doi:https://doi.org/10.1029/2002JD003357.

del Río, C., Lobos, F., Latorre, C., Koch, M., García, J., Osses, P., Lambert, F., Alfaro, F., Siegmund, A., Desert, A., Camilo, Río, D., Cl, 2021. Spatial

distribution and interannual variability of coastal fog and low clouds cover in the hyperarid Atacama Desert and implications for past and present Tillandsia landbeckii ecosystems. Plant Systematics and Evolution 307, 58. doi:10.1007/s00606-021-01782-z.

Scher, H.D., Martin, E.E., 2006. Timing and Climatic Consequences of the Opening of Drake Passage. Science 312, 428–430. doi:10.1126/science.1120044.

Schween, J., Löhnert, U., Westbrook, S., 2022a. Integrated water vapor (IWV TH85) March 2018 - March 2019 at Iquique. URL: https://www.crc1211db.uni-koeln.de/search/view.php?doiID=43. [Accessed 8. April 2023].

Schween, J.H., del Rio, C., García, J.L., Osses, P., Westbrook, S., Löhnert, U., 2022b. Life Cycle of Stratocumulus Clouds over one Year at the Coast of the Atacama Desert. Atmospheric Chemistry and Physics Discussions 2022, 1–33. doi:10.5194/acp-2022-108.

Seely, M., Louw, G., 1980. First approximation of the effects of rainfall on the ecology and energetics of a Namib Desert dune ecosystem. Journal of Arid Environments 3, 25–54. doi:https://doi.org/10.1016/S0140-1963(18)31673-2.

Seidel, D.J., Zhang, Y., Beljaars, A., Golaz, J.C., Jacobson, A.R., Medeiros, B., 2012. Climatology of the planetary boundary layer over the continental United States and Europe. Journal of Geophysical Research: Atmospheres 117. doi:https://doi.org/10.1029/2012JD018143.

Sepulchre, P., Sloan, L.C., Fluteau, F., 2009. Modelling the Response of Amazonian Climate to the Uplift of the Andean Mountain Range. John Wiley & Sons, Ltd. chapter 13. pp. 211–222. doi:https://doi.org/10.1002/9781444306408.ch13.

Serpetzoglou, E., Albrecht, B.A., Kollias, P., Fairall, C.W., 2008. Boundary Layer, Cloud, and Drizzle Variability in the Southeast Pacific Stratocumulus Regime. Journal of Climate 21, 6191 – 6214. doi:10.1175/2008JCLI2186.1.

Sillitoe, R.H., McKee, E.H., 1996. Age of supergene oxidation and enrichment in the Chilean porphyry copper province. Economic Geology 91, 164–179. doi:10.2113/gsecongeo.91.1.164.

Simpson, J., Kummerow, C., Tao, W.K., Adler, R.F., 1996. On the tropical rainfall measuring mission (TRMM). Meteorology and Atmospheric physics 60, 19–36. doi:https://doi.org/10.1007/BF01029783.

Southgate, R.I., Masters, P., Seely, M.K., 1996. Precipitation and biomass changes in the Namib Desert dune ecosystem. Journal of Arid Environments 33, 267–280. doi:10.1006/jare.1996.0064.

Steinke, S., Wahl, S., Crewell, S., 2019. Benefit of high resolution COSMO reanalysis: The diurnal cycle of column-integrated water vapor over Germany. Meteorologische Zeitschrift 28, 165–177. doi:10.1127/metz/2019/0936.

Stubenrauch, C.J., Cros, S., Guignard, A., Lamquin, N., 2010. A 6-year global cloud climatology from the Atmospheric InfraRed Sounder AIRS and a statistical analysis in synergy with CALIPSO and CloudSat. Atmospheric Chemistry and Physics 10, 7197–7214. doi:10.5194/acp-10-7197-2010.

Suzuki, T., 2011. Seasonal variation of the ITCZ and its characteristics over central Africa. Theoretical and Applied Climatology 103, 39–60. doi:10.1007/s00704-010-0276-9.

Tyson, P.D., Preston-Whyte, R.A., 2000. The Weather and Climate of Southern Africa. Second edition ed., Oxford University Press, Oxford, New York.

Vera, C., Baez, J., Douglas, M., Emmanuel, C.B., Marengo, J., Meitin, J., Nicolini, M., Nogues-Paegle, J., Paegle, J., Penalba, O., Salio, P., Saulo, C., Dias, M.A.S., Dias, P.S., Zipser, E., 2006a. The south american low-level jet experiment. Bulletin of the American Meteorological Society 87, 63 – 78. doi:https://doi.org/10.1175/BAMS-87-1-63.

Vera, C., Higgins, W., Amador, J., Ambrizzi, T., Garreaud, R., Gochis, D., Gutzler, D., Lettenmaier, D., Marengo, J., Mechoso, C.R., Nogues-Paegle, J., Dias, P.L.S., Zhang, C., 2006b. Toward a Unified View of the American Monsoon Systems. Journal of Climate 19, 4977 – 5000. doi:10.1175/JCLI3896.1.

Vicencio, J., 2021. Analysis of an extreme precipitation event in the Atacama Desert on January 2020 and its relationship to humidity advection along the Southeast Pacific. Atmósfera 35, 421–448. doi:https://doi.org/10.20937/ATM.52911.

Vuille, M., Bradley, R.S., Werner, M., Keimig, F., 2003. 20th century climate change in the tropical Andes: observations and model results, in: Climate variability and change in high elevation regions: Past, present and future. Springer, pp. 75–99.

Walk, J., Bartz, M., Stauch, G., Binnie, A., Brückner, H., Lehmkuhl, F., 2022. Weathering under coastal hyperaridity – Late Quaternary development of spectral, textural, and gravelometric alluvial fan surface characteristics. Quaternary Science Reviews 277, 107339. doi:https://doi.org/10.1016/j.quascirev.2021.107339.

Wang, Y., Xie, S.P., Xu, H., Wang, B., 2004. Regional Model Simulations of Marine Boundary Layer Clouds over the Southeast Pacific off South America. Part I: Control Experiment. Monthly Weather Review 132, 274 – 296. doi:10.1175/1520-0493(2004)132¡0274:RMSOMB¿2.0.CO;2.

Wang, Y., You, Y., Kulie, M., 2018. Global Virga Precipitation Distribution Derived From Three Spaceborne Radars and Its Contribution to the False Radiometer Precipitation Detection. Geophysical Research Letters 45, 4446–4455. doi:https://doi.org/10.1029/2018GL077891.

Ward, J., Seely, M., Lancaster, N., 1983. On the Antiquity of the Namib. South African Journal of Science 79, 175–183.

Weischet, W., 1975. Las condiciones climáticas del desierto de Atacama como desierto extremo de la tierra. Revista Norte Grande 1, 363–373.

Wood, R., 2012. Stratocumulus clouds. Monthly Weather Review 140, 2373 – 2423. doi:https://doi.org/10.1175/MWR-D-11-00121.1.

Xu, H., Wang, Y., Xie, S.P., 2004. Effects of the Andes on Eastern Pacific Climate: A Regional Atmospheric Model Study. Journal of Climate 17, 589 – 602. doi:10.1175/1520-0442(2004)017¡0589:EOTAOE¿2.0.CO;2.

Zhou, J., Lau, K.M., 1998. Does a Monsoon Climate Exist over South America? Journal of Climate 11, 1020 – 1040. doi:10.1175/1520-0442(1998)011¡1020:DAMCEO¿2.0.CO;2.

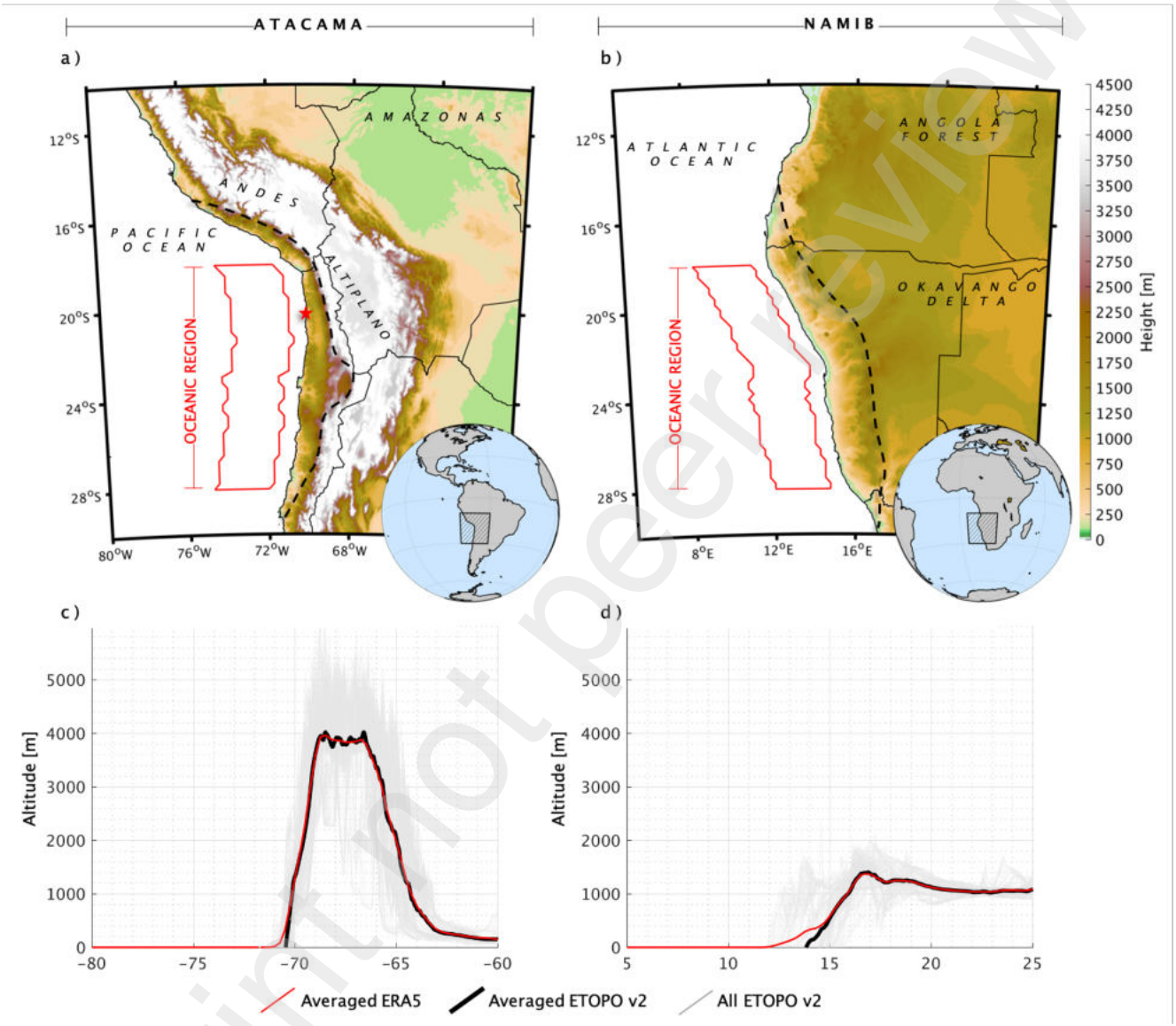

Figure 1: Location of the study area and topographic map of South America and South Africa, with focus on the Atacama (a) and the Namib (b) deserts. Shaded colors represent the height (m ASL). Black dashed lines enclose the deserts. In (c,d) altitude profile (m ASL) over longitude (°E) averaged between 18-28°S according to ETOPOv2 (black line) and ERA5 (red line). Gray thin lines represent topographic profiles at latitudinal intervals of 0.1°.

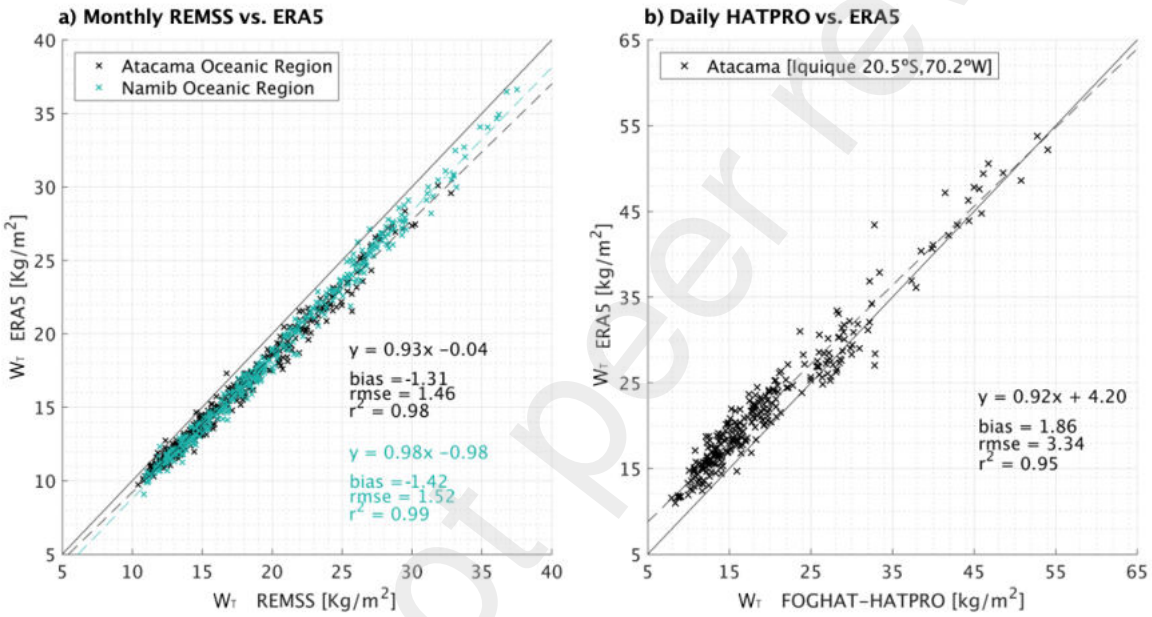

Figure 2: Scatter plot of (a) concurrent monthly values (January 1988-December 2020) of W_T from REMSS and ERA5 for the Atacama Oceanic Region (black cross) and the Namib Oceanic Region (green cross). The linear regression is plotted in dashed lines. In (b), concurrent daily values (March 2018-March 2019) of W_T between HATPRO and ERA5 for Iquique (20.5°S, 70.2°W). In both panels, we included the regression equation, bias, RMSE and R^2.

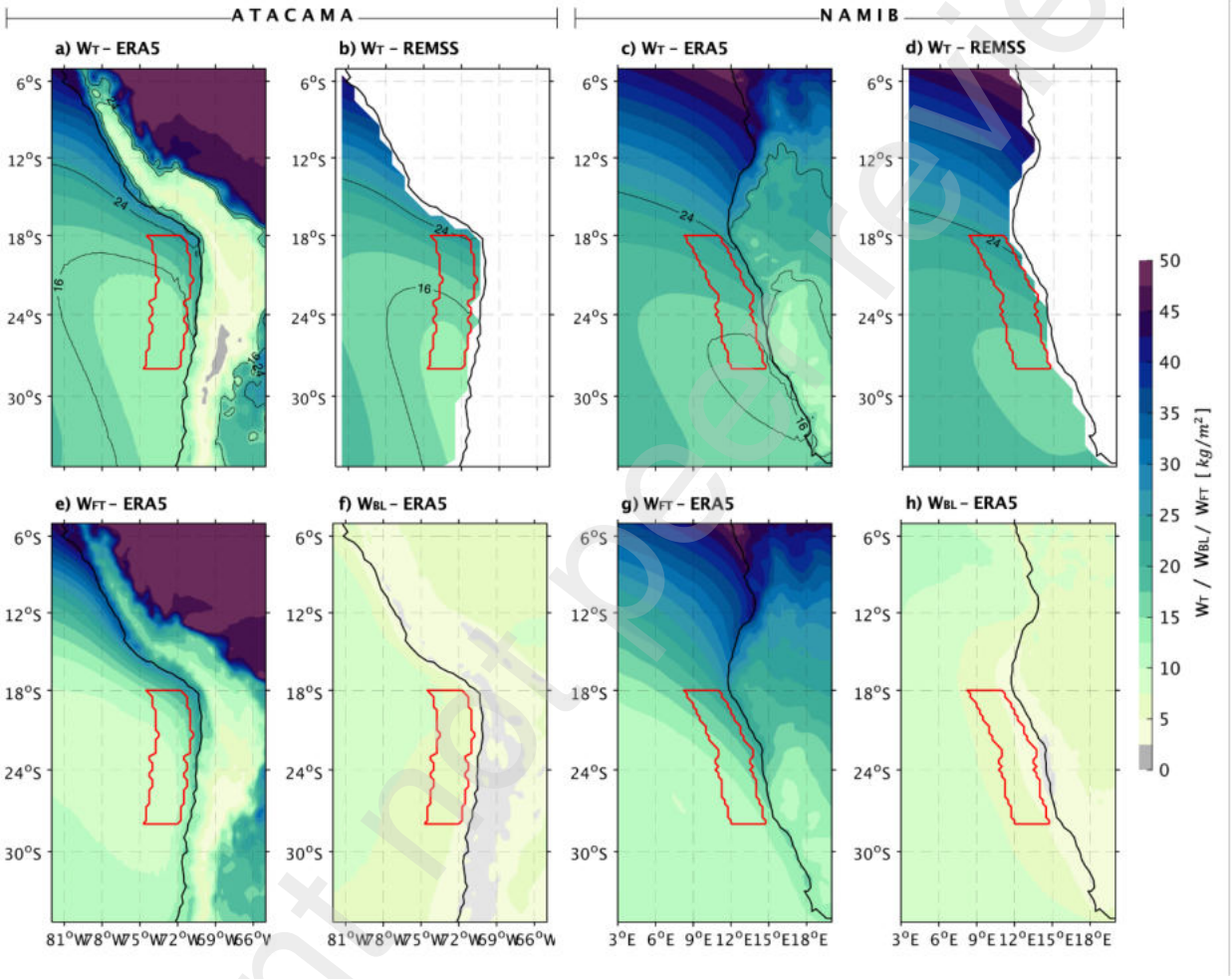

Figure 3: Climatological yearly average of W_T from ERA5 (a,c) and REMSS (b,d), as well as W_{BL} (e,g) and W_{FT} (f,h) from ERA5. Lefts panels are for the Atacama (a,b,e,f) and right panels for the Namib (c,d,g,h). The averages were computed for the period 1988-2020.

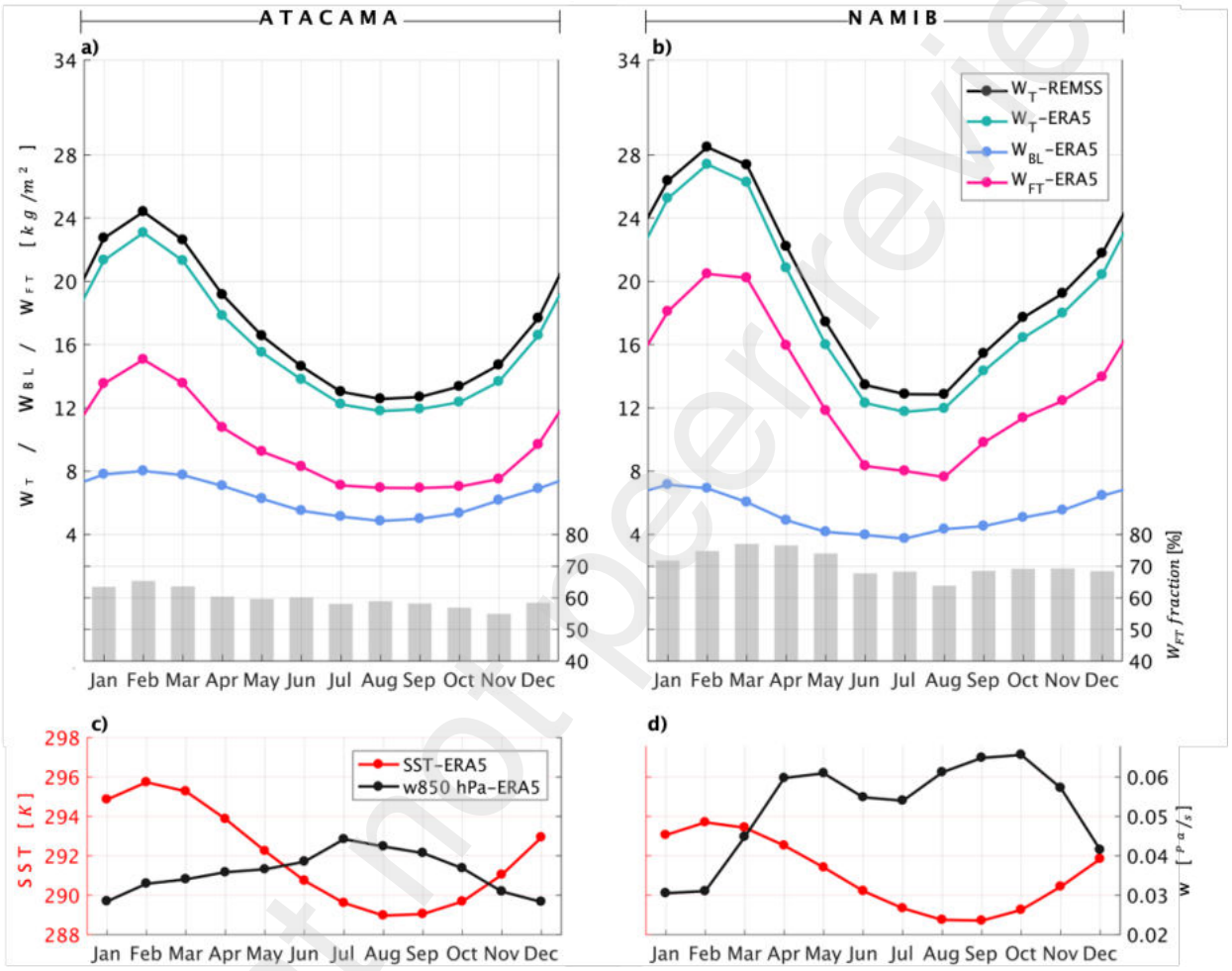

Figure 4: (a,b) Seasonal cycle of the monthly averages of W_T from REMSS (black line) and ERA5 (green line), as well as W_{FT} (magenta lines) and W_{BL} (blue lines) from ERA5. The fraction of W_{FT} with respect to the total column water vapor (in percentage) is presented in gray bars in a and b. (c,d) Seasonal cycless of the SST and w in 850 hPa from ERA5. Left panels are for the Atacama (a,c) and right panels for the Namib (b,d) Oceanic Regions. The averages were computed for the period 1988-2020.

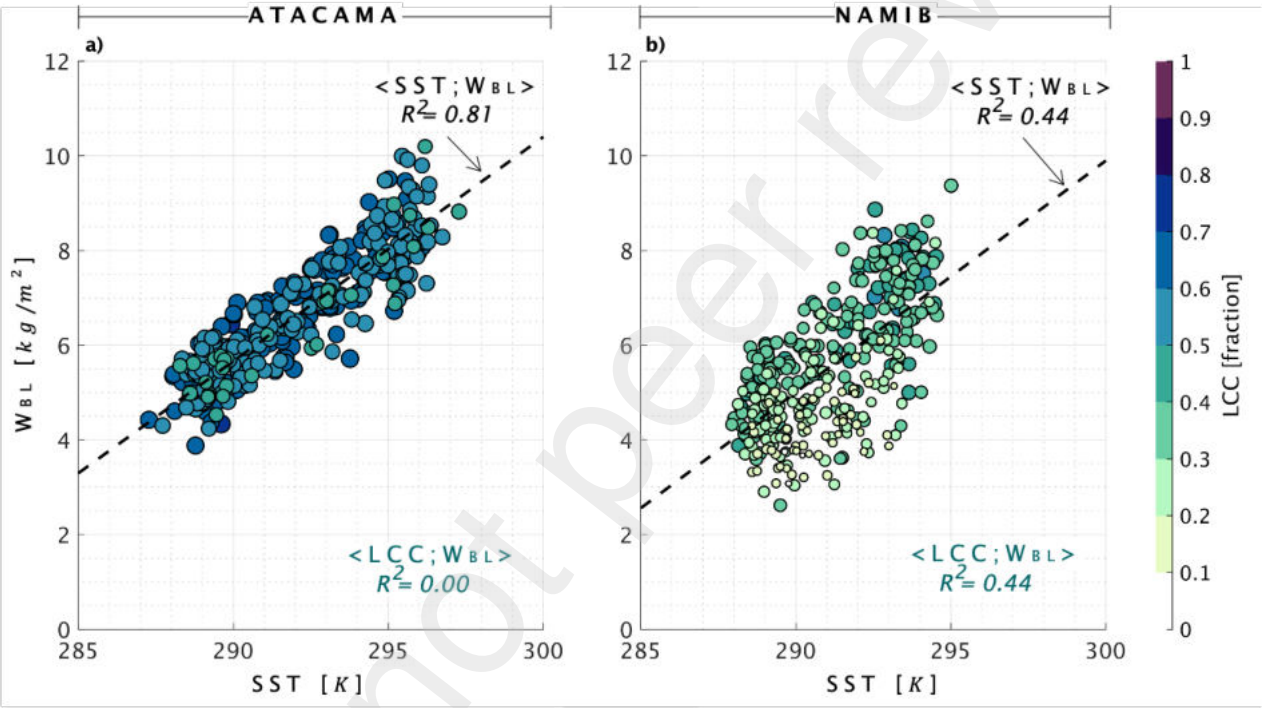

Figure 5: Scatter plot of monthly SST-W_{BL} pairs for the Atacama Oceanic Region (a) and the Namib Oceanic Region (b) between 1988 and 2020 (396 concurrent values). The dashed black line marks the best linear fit. SST-W_{BL} R^2 are annotated at the top right, respectively. The color of the filled circle, as well as the size of the marker, represents the LCC. LCC-W_{BL} R^2 are annotated at the bottom right, respectively. Data from ERA5.

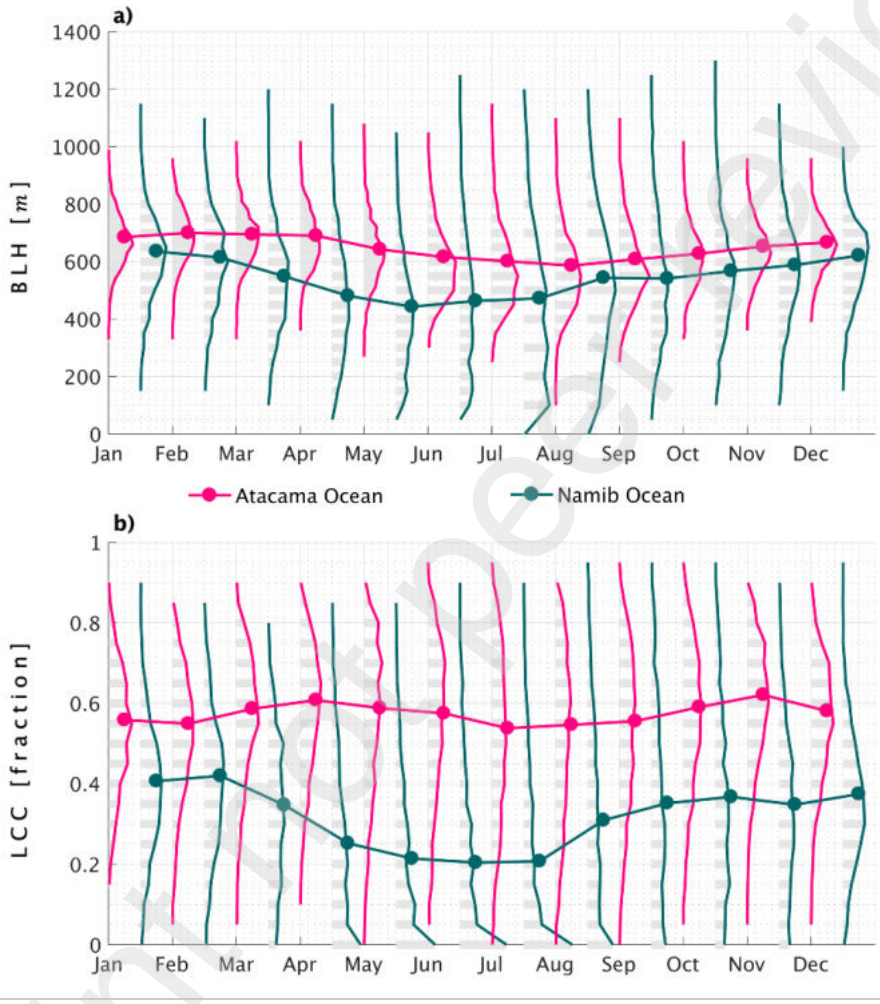

Figure 6: Seasonal cycle of the monthly histograms from daily averages of BLH (a) and LCC (b) for the Atacama Oceanic Region (vertical pink line) and Namib Oceanic Region (vertical green line). The evolution of the monthly means is plotted in the thick horizontal lines with circles. The averages were computed for the period 1988-2020 from ERA5.

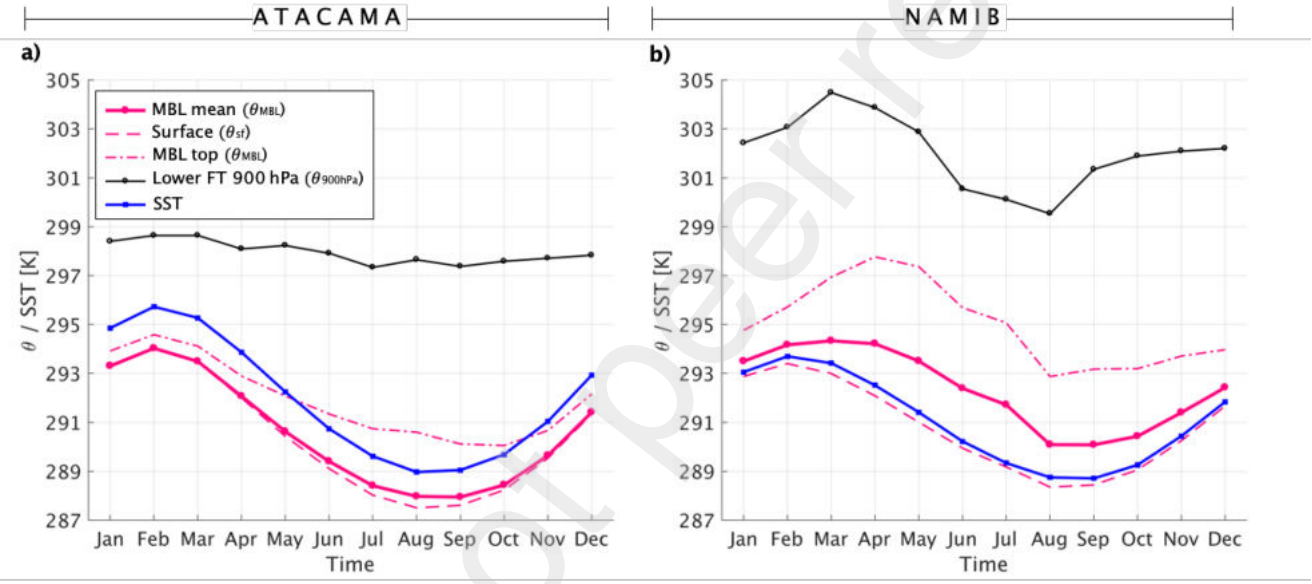

Figure 7: Seasonal cycle of SST (blue line), potential temperature at the surface (θ_{sf}, discontinuous magenta line), at MBL top (θ_{MBL_top}, strip magenta line), the MBL mean (θ_{MBL}, continuous magenta line) and the lower FT at 900 hPa (θ_{900hPa}, black line) for the Atacama Oceanic Region (a) and the Namib Oceanic Region (b). The averages were computed for the period 1988-2020 from ERA5 model level for θ and single level for SST.

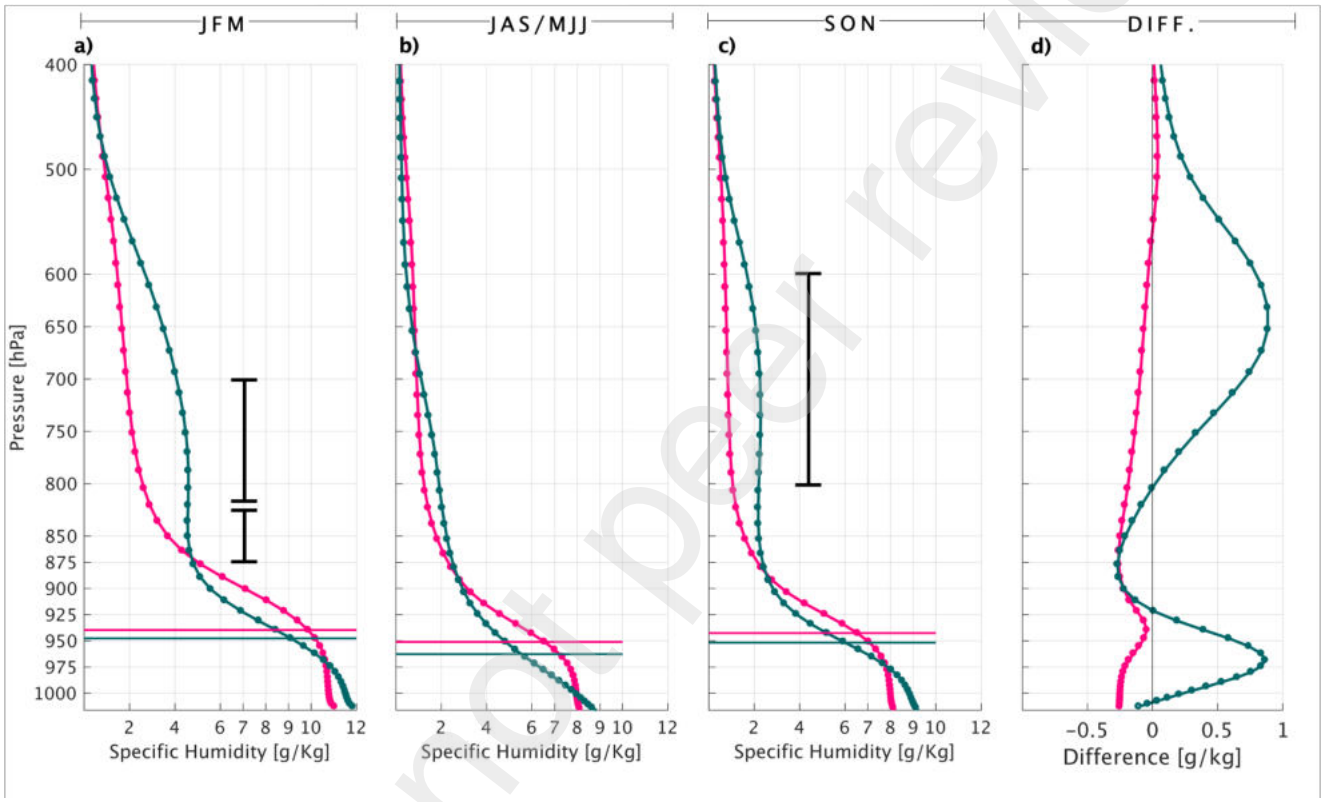

Figure 8: Seasonal vertical profiles of q (g/kg) for the Atacama Oceanic Region (pink line) and Namib Oceanic Region (green line). In (a), the moistest season (JFM), in (b) the driest season of the boundary layer (JAS for the Atacama and MJJ in the Namib), in (c) SON and in (d) the difference SON minus JJA are shown. The horizontal lines represent the altitude of the mean boundary layer height. The vertical black lines represent the areas used for the IVT in Fig. 13. The averages were computed for the period 1988-2020 from ERA5 model levels.

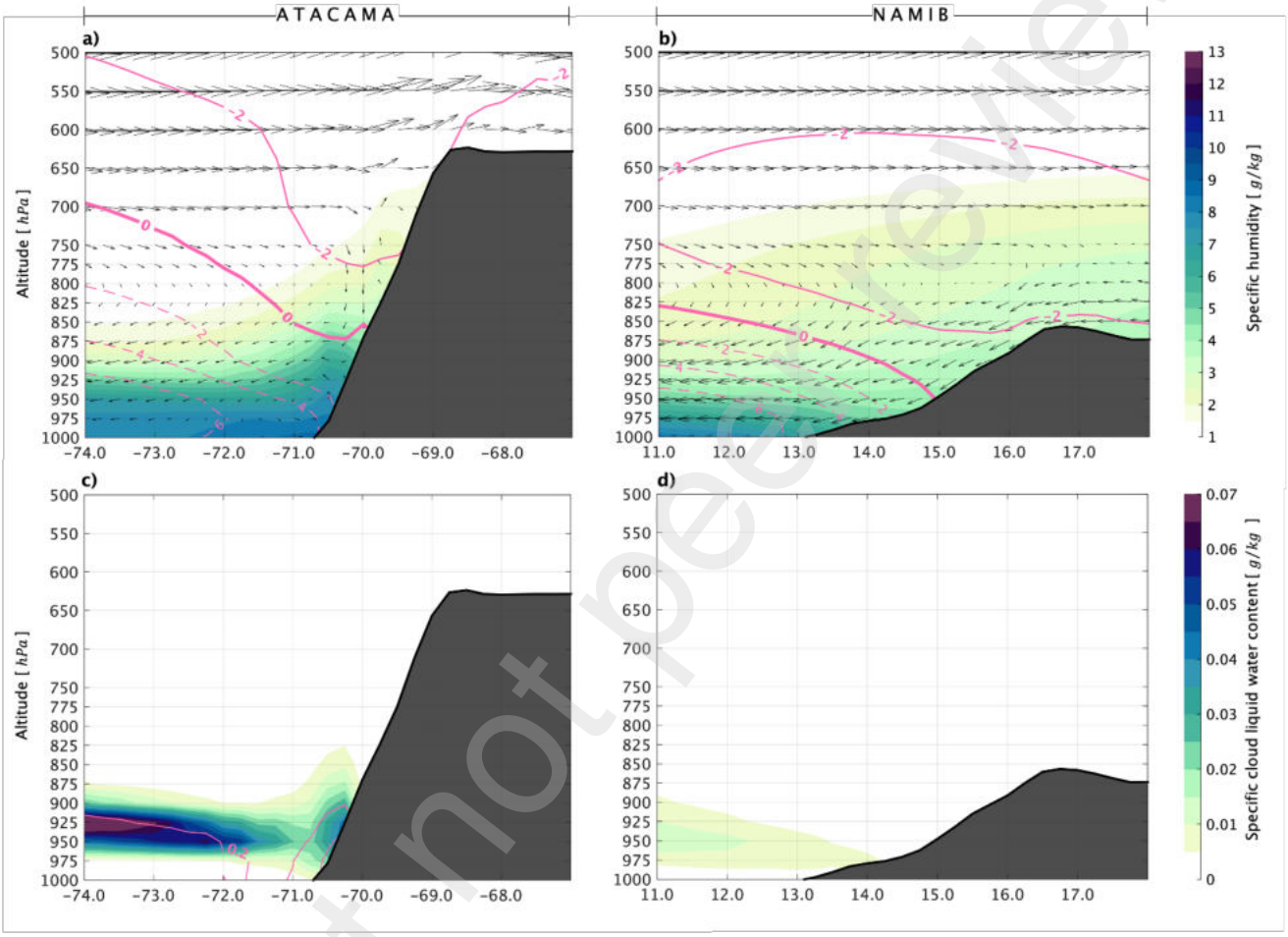

Figure 9: Vertical cross-sections between 18-28°S for the driest season in the boundary layer: JAS in the Atacama (a,c) and MJJ in the Namib (b,d). In the top panels (a,b) q (shaded colors), zonal-vertical winds (arrows, in m/s) and meridional winds (pink contours, dashed lines for positive values) are shown. In the bottom panels (c,d) specific cloud liquid water content (shaded colors), and specific rain liquid water content (pink contours, in 10^6 kg/kg) are shown. The topography is shaded in black. The averages were computed for the period 1988-2020 from ERA5 pressure levels.

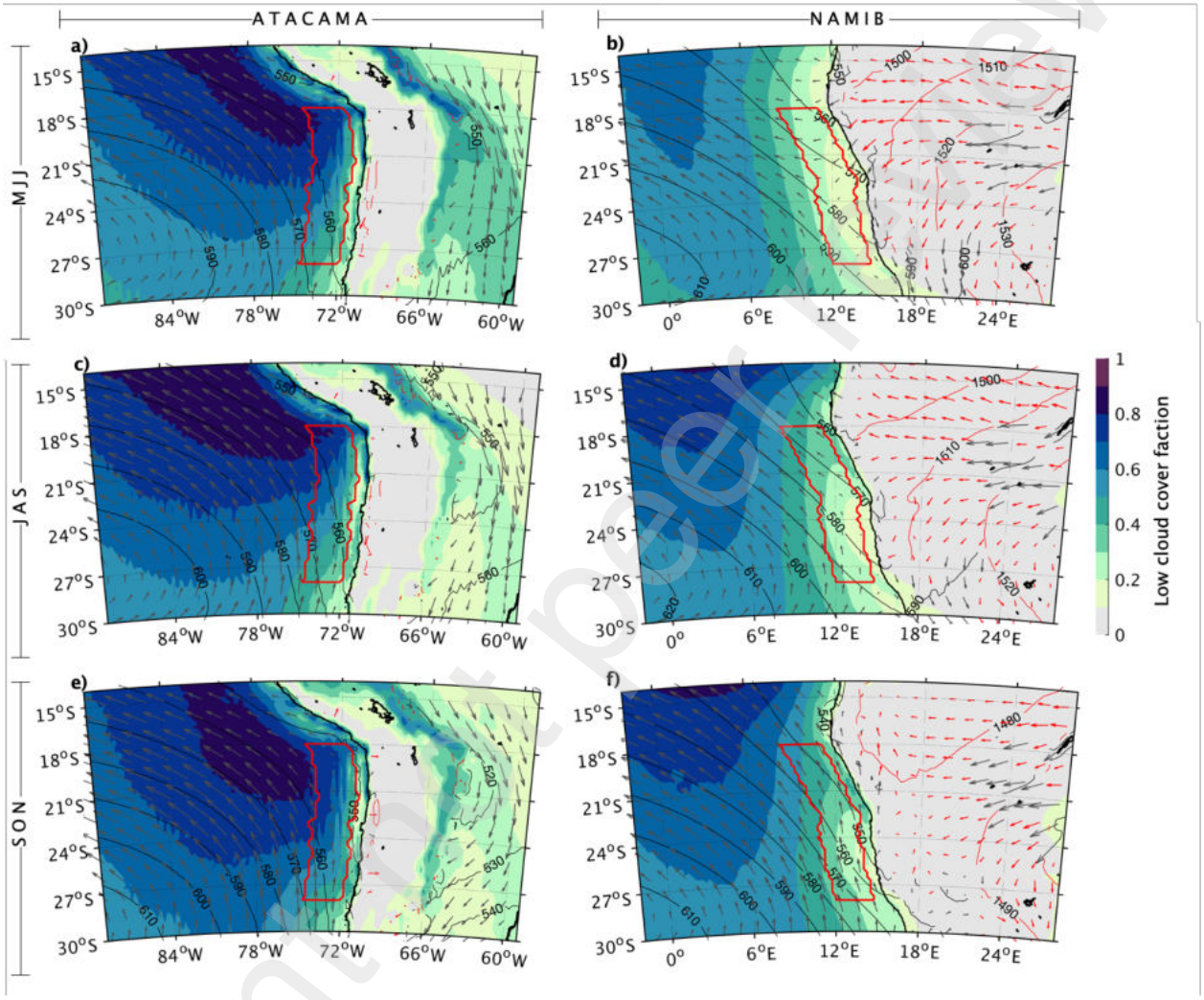

Figure 10: Seasonal composites of LCC (color shading), wind at 950 and 850 hPa (black and red arrows), geopotential height at 950 and 850 hPa (black and red lines) for the Atacama (left panels) and Namib (right panels) and for the next seasons: MJJ (a,b), JAS (c,d) and SON (e,f). The 950 and 850 hPa geopotential/wind field is plotted only for areas where the altitude is <600 m ASL and between 600-1600 m ASL, respectively. The averages were computed for the period 1988-2020 from ERA5 pressure levels.

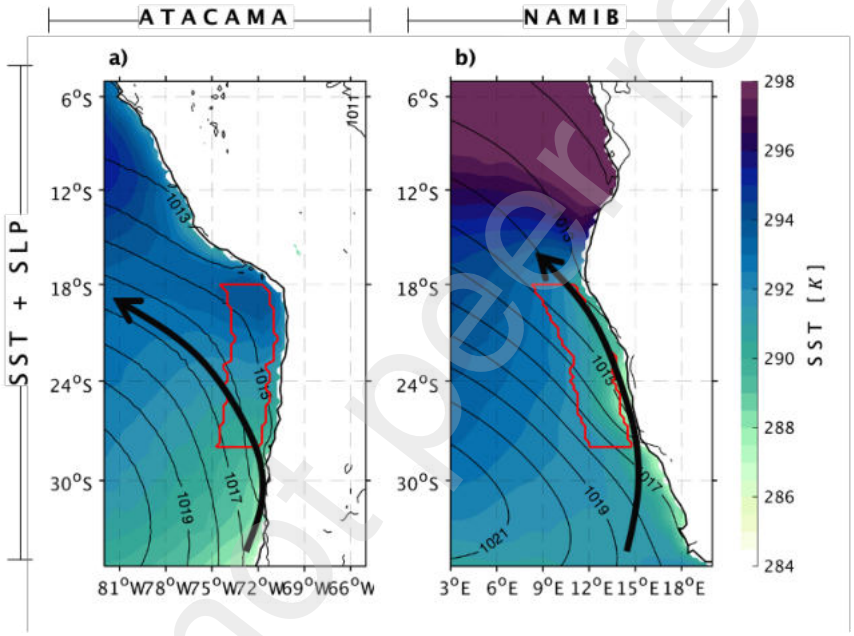

Figure 11: Annual climatological average (1988-2020) of SST (color shading) ad SLP (black contours), for the Atacama (a) and the Namib (b). The approximate location of the Humboldt (a) and Benguela (b) current is indicated by the black arrows following the minimum of SST extending northward. Data from ERA5.

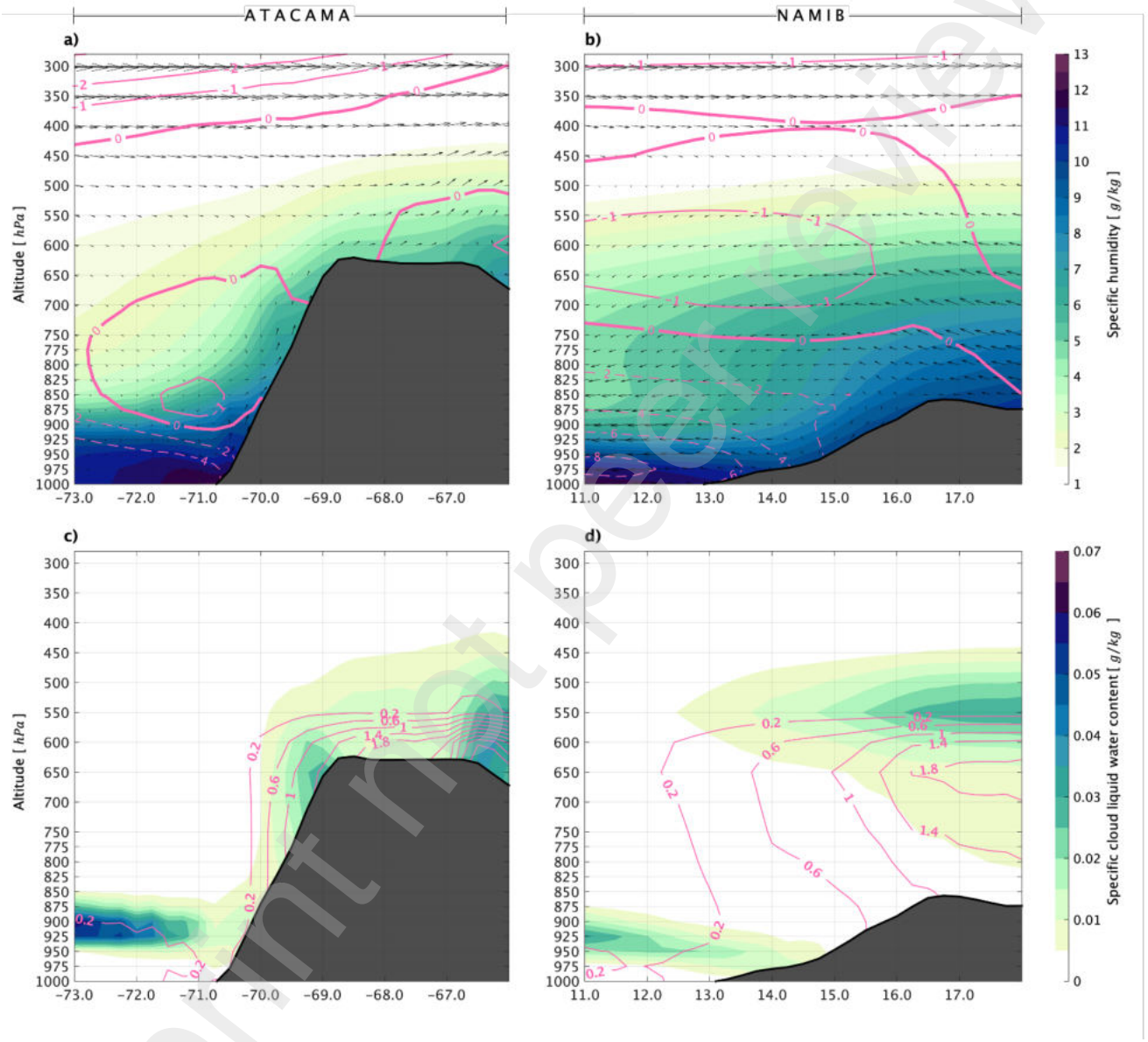

Figure 12: As Figure 9, but for the moistest season in the free-troposphere: JFM for both deserts.

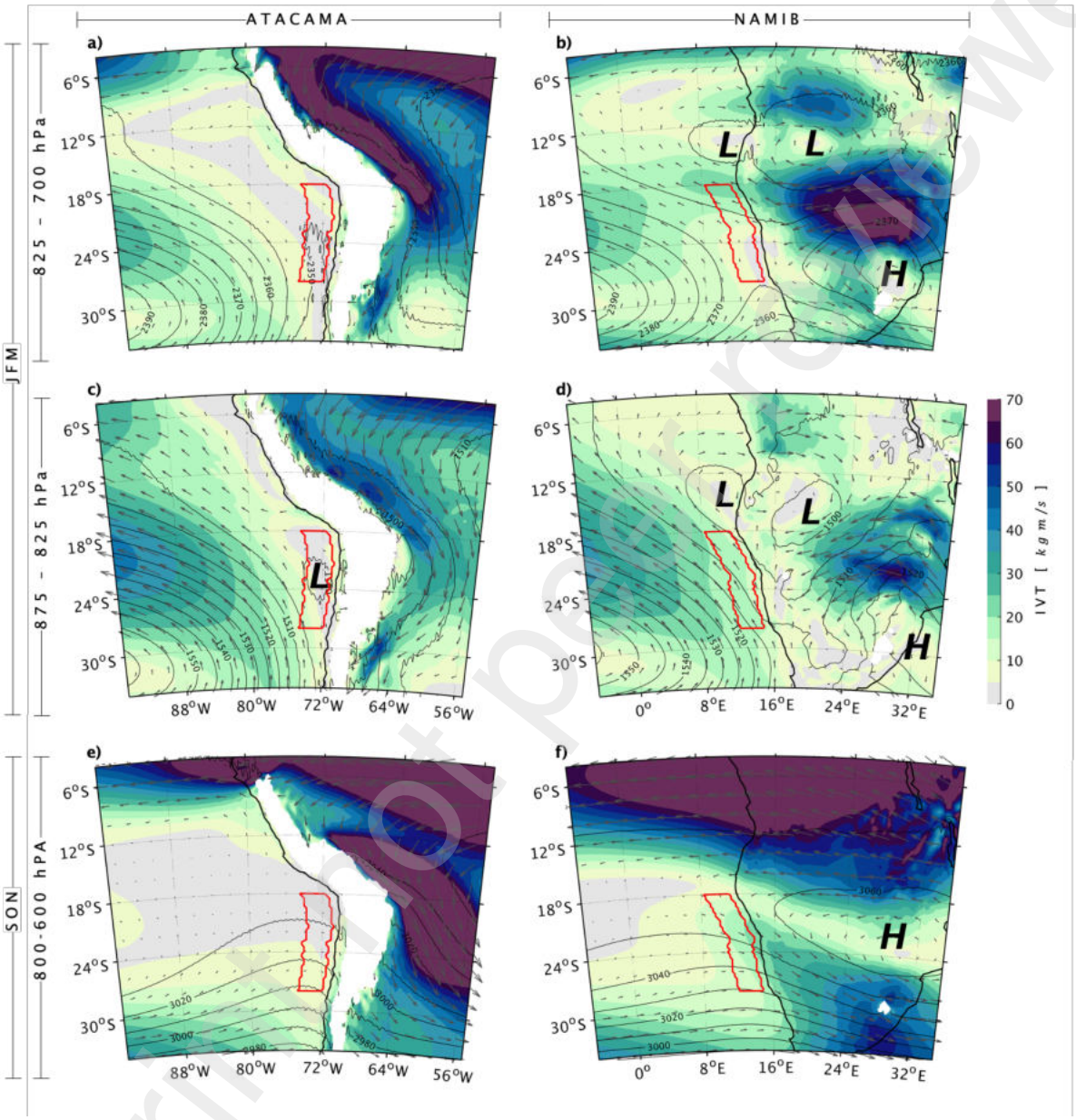

Figure 13: Seasonal composites of the integrated water vapor transport (IVT, black arrows and shaded colors) and geopotential height (black contours) in the Atacama (left panels) and the Namib (right panels). The composites were computed for JFM between 825-700 hPa in the top panels (a,b), JFM and 875-825 hPa in the middle panels (c,d) and for SON between 800-600 hPa in the bottom panels (e,f). The topography is patched white for altitudes under the pressure level of each composite. The averages were computed for the period 1988-2020 from ERA5 pressure levels.

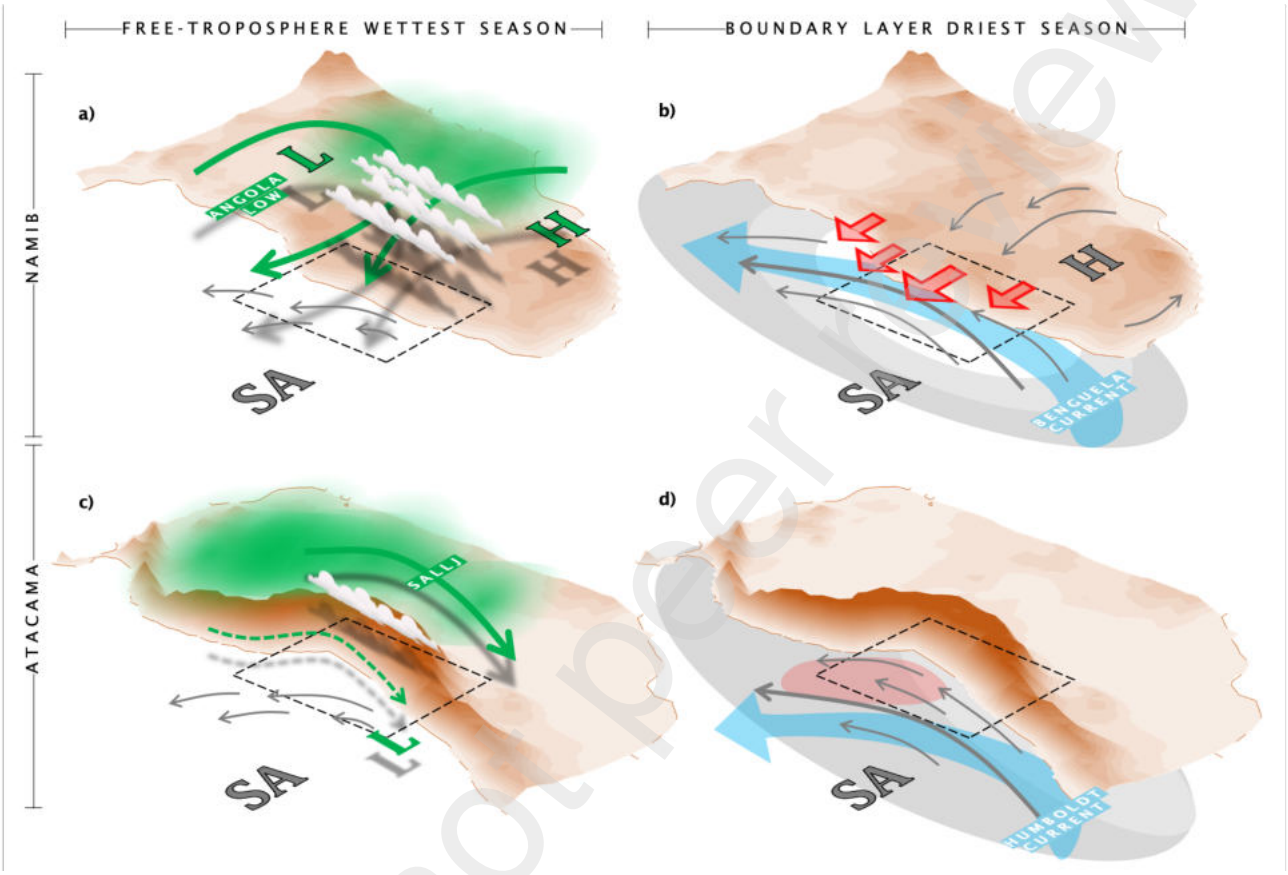

Figure 14: Schematic figure of the main features associated with changes in water vapor and clouds for the moistest season in the free-troposphere (JFM) (a,c) and the driest season in the boundary layer (MJJ for the Namib and JAS for the Atacama) (b,d). In the left panels: circulation pattern at 850 hPa for the Atacama, and between 825-700 hPa in the Namib. Green thick and thin-dashed arrows represent strong and weak water vapor transport, respectively. We included the position of the main low (L) and high (H) pressures systems, as well the South American Low-Level Jet (SALLJ). In the right panels: boundary layer winds are plotted with gray arrows. The stratocumulus cover is represented with gray shades, with darker tones indicating more clouds and white less clouds. The Benguela and Humboldt current are shown by clear blue arrows and warmer SST in clear red. Warmer air in the upper MBL/lower FT is represented by red arrows. We included the position of the Subtropical Anticyclones (SA) and the continental high pressure systems (H).